Kinetic models for imaging in random media

Guillaume Bal [*]   Olivier Pinaud [†]

June 11, 2007

Abstract

We derive kinetic models for the correlations and the energy densities of wave fields propagating in random media. These models take the form of radiative transfer and diffusion equations. We use these macroscopic models to address the detection and imaging of small objects buried in highly heterogeneous media. More specifically, we quantify the influence of small objects on (i) the energy density measured at an array of detectors and (ii) the correlation between the wave field measured in the absence of the object and the wave field measured in the presence of the object. We analyze the advantages and disadvantages of such measurements as a function of the level of disorder in the random media. Numerical simulations verify the theoretical predictions.

1   Introduction

This paper concerns the macroscopic modeling of high frequency waves propagating in highly heterogeneous media. The energy density of classical waves and the probability density of quantum waves in random media have long been modeled by kinetic models such as radiative transfer and diffusion equations [14, 19, 26, 28]. The validity of such approximations was addressed numerically in [8, 25].

Generalizations of these kinetic models were recently considered to model the correlation of two wave fields propagating in two possibly different media; see [4, 10]. Theoretical predictions in [10] on macroscopic models for wave field correlations were confirmed experimentally in [22]. Characterizing such correlations is of interest e.g. in the analysis of the refocusing properties of time-reversed waves -when waves propagating in a heterogeneous medium are recorded and retransmitted into a medium that may have undergone several changes [10]- and in the imaging of changes occurring in the random medium. As an example of application, we consider the imaging of buried inclusions in random media from wave field measurements in the presence and in the

[*]Department of Applied Physics and Applied Mathematics, Columbia University, New York NY, 10027; gb2030@columbia.edu;

[†]Université de Lyon, Université Lyon 1, CNRS, UMR 5208 Institut Camille Jordan/ISTIL, Bâtiment du Doyen Jean Braconnier, 43, blvd du 11 novembre 1918, F - 69622 Villeurbanne Cedex, France; pinaud@math.univ-lyon1.fr

absence of the inclusion. As we shall see, field correlation measurements sometimes allow for more efficient imaging capabilities than with any other type of measurements.

The first contribution of this paper is the validation of radiative transfer equations as accurate macroscopic models for wave energy densities and wave field correlations; see [8]. We also quantify the influence of specific realizations of the random media on the measurements. The radiative transfer equations model the ensemble average of wave energy densities and wave correlations. Even though theoretical analyses [6, 16] predict the statistical stability of the energy densities in the limit of infinite frequencies, frequency is fixed in practical experiments and measurements are somewhat unstable statistically. We quantify this statistical instability numerically.

The second contribution of the paper concerns the imaging of (small volume) inclusions in highly heterogeneous media, when the mean free path characterizing disorder in the medium is too small -whence the medium too strongly scattering- for techniques based on coherent wave field information [11, 12] to be relied upon. Once macroscopic models are available to accurately describe wave propagation, the inclusions may be regarded as local perturbations in the constitutive parameters of the macroscopic equations. Since the volume of the inclusions is typically small compared to the overall size of propagation, small-volume approximations offer accurate descriptions. Following work in [2, 13], we characterize the influence of small volume inclusions in two types of regimes, the transport regime and the diffusion regime, and for two types of measurements, wave energy measurements and wave correlation measurements. The analysis can then be used to image the inclusions as in e.g. [1, 2, 3, 7, 13], which is not considered further here.

The analysis of the validity of the macroscopic models and the analysis of the influence of small volume inclusions allow us to compare several imaging scenarios. In all the imaging scenarios considered here, the realization of the random medium is *not* known exactly. (i) The first and most difficult scenario is when energy density measurements are available only in the presence of the inclusion. We then need to estimate the macroscopic properties of the random medium and image the inclusion at the same time. The influence of the object then needs to be much larger than the error resulting from our lack of knowledge of the realization of the random medium, or equivalently much larger than the aforementioned statistical instability of the energy measurements. (ii) In the second scenario we assume that we have access to the wave energy density in the absence of the inclusion *and* in the presence of the inclusion. These differential measurements allow us to obtain measurements whose magnitude is in some sense proportional to the inclusion. Using a kinematic picture, all the paths that do not visit the inclusion's location do not contribute to the differential measurements since they exactly cancel. Such paths cause most of the statistical instability that hampers imaging in the first scenario. (iii) In the last scenario, we assume access to wave field measurements in the presence and in the absence of the inclusion so that we can form their two-field correlation. Since wave field measurement may be more difficult to evaluate accurately than wave energy density measurements, this scenario is the most demanding technologically. It will prove however extremely valuable in imaging in very scattering underlying media.

The rest of the paper is structured as follows. Section 2 presents the radiative transfer and diffusion equations to model wave energy densities. These models are generalized to account for the correlation of wave fields in the presence and in the absence of the

2

inclusion. Here, an inclusion is modeled by a (possibly regularized) jump in the sound speed and possibly by a suppression of the heterogeneous fluctuations. The details in the derivation of the kinetic model are given in Appendix A.

The influence of small volume inclusions is modeled in Section 3. We obtain different orders of magnitude for the inclusion's influence depending on the regime of wave propagation, radiative transfer or diffusion, and on the type of measurements, energy densities or wave field correlations. Some details of the derivation are postponed to Appendix B. Section 4 analyzes the three imaging scenarios described above and compares them in the transport and diffusion regimes of wave propagation.

The validity of the transport models is addressed numerically in Section 5. We perform wave field propagation over a two-dimensional domain of size equal to 200×200 wavelengths and compare wave energy and wave field correlation measurements with kinetic model predictions. The kinetic equations are solved by using a Monte Carlo method. We also estimate the statistical instability of the energy density measurements as a function of the size of the array of detectors. This information is important in imaging based on the first scenario. Section 6 offers some concluding remarks.

2   Macroscopic kinetic models

In this section, we recall the transport and diffusion equations that model high frequency wave propagation in highly heterogeneous media. We then adapt the macroscopic models to account for localized changes in the random media. These changes model here the presence of a small inclusion. Small means small with respect to the overall distance of propagation. We shall see that the objects have to be large compared to the typical wavelength of the wave fields in order to be detectable.

2.1   High frequency regime

We consider here scalar (acoustic) waves for concreteness. Generalization to other classical waves may be done as in e.g. [4, 26]. Wave propagation may thus be described by the following second-order equation:

$$\frac{\partial^2 p}{\partial t^2} = \kappa^{-1}(\mathbf{x})\nabla \cdot \rho^{-1}(\mathbf{x})\nabla p, \qquad \mathbf{x} \in \mathbb{R}^d,\ t > 0, \tag{1}$$

supplemented with initial conditions $p(t = 0, \mathbf{x})$ and $\frac{\partial p}{\partial t}(t = 0, \mathbf{x})$. Here, p is acoustic pressure and ρ and κ are density and compressibility of the underlying media, respectively. We shall assume that $\rho(\mathbf{x}) = \rho_0$ is constant to simplify the presentation. All the kinetic models derived in this paper are readily generalized to the case of a non-constant density.

In the high-frequency regime, rescaling time and space as $t \to \varepsilon t$ and $\mathbf{x} \to \varepsilon \mathbf{x}$, the wave equation is recast as:

$$\frac{\partial^2 p^\varepsilon}{\partial t^2} = c_\varepsilon^2(\mathbf{x})\Delta p^\varepsilon, \tag{2}$$

with the same initial conditions at $t = 0$ and where $c_\varepsilon(\mathbf{x}) := (\rho_0 \kappa_\varepsilon(\mathbf{x}))^{-1/2}$ with

$$\kappa_\varepsilon(\mathbf{x}) = \kappa_0 + \sqrt{\varepsilon}\kappa_1\left(\frac{\mathbf{x}}{\varepsilon}\right),$$

where κ_0 is the background compressibility (assumed to be constant to simplify) and κ_1 accounts for the random fluctuations. The strength of the fluctuations is weak and of order $\sqrt{\varepsilon}$. Since the length scale of the fluctuations is of order ε, waves still encounter on the order of $\varepsilon^{-1/2} \gg 1$ "fluctuations" when propagating for a distance of order $L = O(1)$.

A systematic derivation of radiative transfer models for wave propagation in random media was developed in [26]. To avoid complications caused by the presence of vortical (non-propagating) acoustic modes, we recast the wave equation as a two-by-two system of equations and follow the equivalent method presented in [4]. Let us introduce the quantity

$$q^\varepsilon(t, \mathbf{x}) = \frac{\varepsilon}{c_\varepsilon^2(\mathbf{x})} \frac{\partial p^\varepsilon}{\partial t}(t, \mathbf{x}). \tag{3}$$

The wave equation may then be recast as the following hyperbolic first-order system of equations for $\mathbf{u}_\varepsilon = (p^\varepsilon, q^\varepsilon)$:

$$\varepsilon \frac{\partial \mathbf{u}_\varepsilon}{\partial t} + A_\varepsilon \mathbf{u}_\varepsilon = 0, \qquad \mathbf{x} \in \mathbb{R}^d,\ t > 0, \tag{4}$$

where A_ε is given by

$$A_\varepsilon = - \begin{pmatrix} 0 & c_\varepsilon^2(\mathbf{x}) \\ \varepsilon^2 \Delta & 0 \end{pmatrix}. \tag{5}$$

Based on our assumptions on $\kappa_\varepsilon(\mathbf{x})$, we have, up to negligible lower order terms in ε, that

$$c_\varepsilon^2(\mathbf{x}) = c_0^2 - \sqrt{\varepsilon} V\left(\frac{\mathbf{x}}{\varepsilon}\right), \qquad c_0^2 = \frac{1}{\rho_0 \kappa_0}, \qquad V(\mathbf{y}) = \frac{c_0^2}{\kappa_0} \kappa_1(\mathbf{y}). \tag{6}$$

All of the heterogeneity of the underlying medium is thus encoded into $\kappa_1(\mathbf{x})$ or equivalently $V(\mathbf{x})$. We assume that $V(\mathbf{x})$ is a mean-zero, homogeneous stationary random field. All we need to know about the random field at the kinetic (macroscopic) level is its two point correlation $R(\mathbf{x})$. The power spectrum of V is the Fourier transform of $R(\mathbf{x})$ and we have the following relations:

$$\begin{aligned} c_0^4 R(\mathbf{y}) &= \mathbb{E}\{V(\mathbf{x})V(\mathbf{x}+\mathbf{y})\}, \\ (2\pi)^d c_0^4 \hat{R}(\mathbf{p})\delta(\mathbf{p}+\mathbf{q}) &= \mathbb{E}\{\hat{V}(\mathbf{p})\hat{V}(\mathbf{q})\}, \end{aligned} \tag{7}$$

where $\hat{V}(\mathbf{p})$ denotes the Fourier transform of $V(\mathbf{y})$ and $\mathbb{E}$ denotes ensemble average over the fluctuations.

When an inclusion is present in the random medium, the properties of the underlying media are perturbed locally. We assume here that the inclusion is modeled by a sound speed $c_1^2 = c_0^2 + \Delta c^2 > 0$ that is different from the surrounding environment and constant. Equivalently, the inclusion is modeled as a local change in the compressibility $\kappa_0 + \Delta\kappa > 0$ so that $\Delta c^2 = -c_0^2 \frac{\Delta\kappa}{\kappa_0 + \Delta\kappa}$. We denote by Ω the support of the inclusion. In the presence of an inclusion, the sound speed thus need be modified as

$$c_\varepsilon^2(\mathbf{x}) = c_0^2 + \chi(\mathbf{x})\Delta c^2 - \sqrt{\varepsilon}(1 - \gamma\chi(\mathbf{x}))V(\frac{\mathbf{x}}{\varepsilon}), \tag{8}$$

where $\chi(\mathbf{x}) = 1$ for $\mathbf{x} \in \Omega$ and $\chi(\mathbf{x}) = 0$ elsewhere. Here γ is a parameter modeling fluctuations within the inclusion, with $\gamma = 1$ if random fluctuations are suppressed

within the inclusion and $\gamma = 0$ if fluctuations are still present within the inclusion and have the same statistics as outside of the inclusion.

To distinguish the fields propagating in the unperturbed and perturbed media, we denote them by $\mathbf{u}_\varepsilon^1 = (p_\varepsilon^1, q_\varepsilon^1)$ and $\mathbf{u}_\varepsilon^2 = (p_\varepsilon^2, q_\varepsilon^2)$, respectively. They satisfy the following systems of equations:

$$\varepsilon \frac{\partial \mathbf{u}_\varepsilon^\varphi}{\partial t} + A_\varepsilon^\varphi \mathbf{u}_\varepsilon^\varphi = 0, \qquad \varphi = 1, 2, \quad \mathbf{x} \in \mathbb{R}^d, \quad t > 0,$$

$$A_\varepsilon^\varphi = - \begin{pmatrix} 0 & c_0^2 \\ \varepsilon^2 \Delta & 0 \end{pmatrix} + V_\varepsilon^\varphi(\mathbf{x}, \frac{\mathbf{x}}{\varepsilon}) K, \qquad K = \begin{pmatrix} 0 & 1 \\ 0 & 0 \end{pmatrix},$$

$$V_\varepsilon^1(\mathbf{x}, \frac{\mathbf{x}}{\varepsilon}) := V_\varepsilon^1(\frac{\mathbf{x}}{\varepsilon}) = \sqrt{\varepsilon} V(\frac{\mathbf{x}}{\varepsilon}),$$

$$V_\varepsilon^2(\mathbf{x}, \frac{\mathbf{x}}{\varepsilon}) = \chi(\mathbf{x}) \Delta c^2 + \sqrt{\varepsilon}(1 - \gamma \chi(\mathbf{x})) V(\frac{\mathbf{x}}{\varepsilon}).$$

The relevant macroscopic quantities we wish to consider are the energy densities $\mathcal{E}^\varepsilon(t, \mathbf{x})$ in the absence and $\mathcal{E}_{\mathrm{inc}}^\varepsilon(t, \mathbf{x})$ in the presence of an inclusion and the cross-correlation $\mathcal{C}^\varepsilon(t, \mathbf{x})$ of the two wave fields. They are defined by

$$\begin{aligned}
\mathcal{E}^\varepsilon(t, \mathbf{x}) &= \tfrac{1}{2} \left(\kappa_0 \, (p_\varepsilon^1(t, \mathbf{x}))^2 + \rho_0 |\mathbf{v}_\varepsilon^1(t, \mathbf{x})|^2 \right), \\
\mathcal{E}_{\mathrm{inc}}^\varepsilon(t, \mathbf{x}) &= \tfrac{1}{2} \left(\kappa_2(\mathbf{x}) \, (p_\varepsilon^2(t, \mathbf{x}))^2 + \rho_0 |\mathbf{v}_\varepsilon^2(t, \mathbf{x})|^2 \right), \\
\mathcal{C}^\varepsilon(t, \mathbf{x}) &= \tfrac{1}{2} \left(\kappa_0^{\frac{1}{2}} \kappa_2^{\frac{1}{2}}(\mathbf{x}) p_\varepsilon^1(t, \mathbf{x}) \, p_\varepsilon^2(t, \mathbf{x}) + \rho_0 \mathbf{v}_\varepsilon^1(t, \mathbf{x}) \cdot \mathbf{v}_\varepsilon^2(t, \mathbf{x}) \right),
\end{aligned} \tag{9}$$

where $\kappa_2(\mathbf{x}) = \kappa_0 + \Delta \kappa \, \chi(\mathbf{x})$ and $\mathbf{v}_\varepsilon^i$ is defined via the relation $q_\varepsilon^i = -\rho_0 \nabla \cdot \mathbf{v}_\varepsilon^i$. We now consider the evolution of these quantities in the radiative transfer regime.

2.2 Transport equations

The macroscopic description of the energy density $\mathcal{E}^\varepsilon(t, \mathbf{x})$ in (9) is quite standard and may be found in e.g. [4, 24, 26]. The asymptotic behaviors of $\mathcal{E}_{\mathrm{inc}}^\varepsilon(t, \mathbf{x})$ and $\mathcal{C}^\varepsilon(t, \mathbf{x})$ in the high frequency regime, i.e., mathematically as $\varepsilon \to 0$, are the main contributions of this section. These behaviors are obtained following the methodology developed in [4, 10].

In the regime of radiative transfer, the physical energy densities $\mathcal{E}^\varepsilon(t, \mathbf{x})$ and $\mathcal{E}_{\mathrm{inc}}^\varepsilon(t, \mathbf{x})$ and the correlation $\mathcal{C}^\varepsilon(t, \mathbf{x})$ do not satisfy closed-form equations. The energy density need be modeled in the space of positions and momenta by means of the following Wigner transform

$$\begin{aligned}
W_\varepsilon^{j,k}(t, \mathbf{x}, \mathbf{k}) &= W \left[\mathbf{u}_\varepsilon^j(t, \cdot), \mathbf{u}_\varepsilon^k(t, \cdot) \right] (\mathbf{x}, \mathbf{k}), \\
&= \int_{\mathbb{R}^d} e^{i \mathbf{k} \cdot \mathbf{y}} \, \mathbf{u}_\varepsilon^j(t, \mathbf{x} - \frac{\varepsilon \mathbf{y}}{2}) \left(\mathbf{u}_\varepsilon^k \right)^* (t, \mathbf{x} + \frac{\varepsilon \mathbf{y}}{2}) \frac{d\mathbf{y}}{(2\pi)^d},
\end{aligned} \tag{10}$$

for $1 \le j, k \le 2$. It is shown formally in the aforementioned references that $W_\varepsilon^j := W_\varepsilon^{j,j}$ converges as $\varepsilon \to 0$ to a limiting Wigner measure

$$W_0^j(t, \mathbf{x}, \mathbf{k}) = a_+^j(t, \mathbf{x}, \mathbf{k}) \mathbf{b}_+^j(\mathbf{x}, \mathbf{k}) \mathbf{b}_+^j(\mathbf{x}, \mathbf{k})^* + a_-^j(t, \mathbf{x}, \mathbf{k}) \mathbf{b}_-^j(\mathbf{x}, \mathbf{k}) \mathbf{b}_-^j(\mathbf{x}, \mathbf{k})^*,$$

where we have defined

$$\mathbf{b}^1_\pm(\mathbf{k}) = \frac{1}{\sqrt{2}}\begin{pmatrix} \pm i|\mathbf{k}| \\ c_0^{-1} \end{pmatrix}, \quad \mathbf{b}^2_\pm(\mathbf{x}, \mathbf{k}) = \frac{1}{\sqrt{2}}\begin{pmatrix} \pm i|\mathbf{k}| \\ (c(\mathbf{x}))^{-1} \end{pmatrix}, \quad c(\mathbf{x}) = \left(c_0^2 + \chi(\mathbf{x})\Delta c^2\right)^{\frac{1}{2}}.$$

In the absence of an inclusion, the amplitude of the propagating mode a^1_+ solves the following radiative transfer equation:

$$\frac{\partial a^1_+}{\partial t} + c_0\,\hat{\mathbf{k}}\cdot\nabla_{\mathbf{x}}a^1_+ + \Sigma(\mathbf{k})\,a^1_+ = Q(a^1_+), \qquad \mathbf{x}\in\mathbb{R}^d, \tag{11}$$

augmented with prescribed initial conditions $a^1_+(0, \mathbf{x}, \mathbf{k})$, where $\hat{\mathbf{k}} = \frac{\mathbf{k}}{|\mathbf{k}|}$ and where Q and Σ^{-1} denote the collision operator and mean free time, respectively, and are given by:

$$Q(a) = \int_{\mathbb{R}^d} a(t, \mathbf{x}, \mathbf{p})\sigma(\mathbf{k}, \mathbf{p})\delta(c_0|\mathbf{p}| - c_0|\mathbf{k}|)d\mathbf{p}, \qquad \Sigma(\mathbf{k}) = \int_{\mathbb{R}^d}\sigma(\mathbf{k}, \mathbf{p})\delta(c_0|\mathbf{p}| - c_0|\mathbf{k}|)d\mathbf{p}. \tag{12}$$

The cross section $\sigma(\mathbf{k}, \mathbf{p})$ appearing in these expressions is given by

$$\sigma(\mathbf{k}, \mathbf{p}) = \frac{\pi c_0^2|\mathbf{k}|^2}{2(2\pi)^d}\hat{R}(\mathbf{k} - \mathbf{p}). \tag{13}$$

A similar expression is obtained for $a^1_-(t, \mathbf{x}, \mathbf{k}) = a^1_+(t, \mathbf{x}, -\mathbf{k})$. The physical energy density is then derived from the phase-space energy density by averaging out the momenta variable:

$$\lim_{\varepsilon\to 0}\mathcal{E}^\varepsilon(t, \mathbf{x}) = \int_{\mathbb{R}^d} a^1_+(t, \mathbf{x}, \mathbf{k})d\mathbf{k}. \tag{14}$$

The energy density a^1_+ is a uniquely defined deterministic quantity. In the limit of high frequencies, the energy densities are thus self-averaging, in the sense that they depend on the statistics of the random medium and not on its specific realization. This is good news as they are stable observables and thus are useful in imaging. How stable the energy is at a small but non-vanishing ε remains an important question that will be addressed numerically in Section 5.

The rest of this section is devoted to the derivation of macroscopic models for $\mathcal{E}^\varepsilon_{\text{inc}}(t, \mathbf{x})$ and $\mathcal{C}^\varepsilon(t, \mathbf{x})$. The details of the derivations are postponed to Appendix A.

Energy density in the presence of an inclusion. We now generalize the above kinetic model to obtain a description of the energy density $\mathcal{E}^\varepsilon_{\text{inc}}(t, \mathbf{x})$ in the presence of an inclusion. As in (14), the physical energy density $\mathcal{E}^\varepsilon_{\text{inc}}$ may be decomposed in the phase space as:

$$\lim_{\varepsilon\to 0}\mathcal{E}^\varepsilon_{\text{inc}}(t, \mathbf{x}) = \int_{\mathbb{R}^d} a^2_+(t, \mathbf{x}, \mathbf{k})d\mathbf{k}. \tag{15}$$

We need to find an equation for $a^2_+(t, \mathbf{x}, \mathbf{k})$. The derivation of the kinetic model from (10) to (11) is local in nature. This means that that limit of $W\left[\phi(\mathbf{x})\mathbf{u}^j_\varepsilon(t, \cdot), \phi(\mathbf{x})\mathbf{u}^k_\varepsilon(t, \cdot)\right](\mathbf{x}, \mathbf{k})$ is $|\phi(\mathbf{x})|^2$ times the limit of $W\left[\mathbf{u}^j_\varepsilon(t, \cdot), \mathbf{u}^k_\varepsilon(t, \cdot)\right](\mathbf{x}, \mathbf{k})$, where $\phi(\mathbf{x})$ is an arbitrary smooth test function; see [17] for the details. As a consequence, $a^2_+(t, \mathbf{x}, \mathbf{k})$ solves (11) for $\mathbf{x}\in\mathbb{R}^d\backslash\bar{\Omega}$.

6

For the same reasons, $a_+^2(t, \mathbf{x}, \mathbf{k})$ solves a radiative transfer equation of the form (11) with c_0^2 replaced by $c_1^2 = c_0^2 + \Delta c^2$ and Q replaced by $(1-\gamma)Q$ for $\mathbf{x} \in \Omega$, i.e., inside the inclusion. The parameter γ introduced in (8) measures the amount of random fluctuations inside the inclusion (with $\gamma = 1$ corresponding to a suppression of the random fluctuations inside the inclusion).

It remains to link the energy densities $a_+^2(t, \mathbf{x}, \mathbf{k})$ across the interface $\partial\Omega$. In the case of a sharp jump of the velocity field $c(\mathbf{x}) = c_0$ for $\mathbf{x}$ outside of Ω and $c(\mathbf{x}) = c_1$ inside Ω, wave fields impinging upon the interface $\partial\Omega$ are partially reflected and partially transmitted according to the classical Snell-Descartes laws. These laws directly translate into equivalent reflection and transmission conditions for the wave energy density at the inclusion's boundary. Because we shall not use such interface conditions any further in the paper, we refer the interested reader to [5] for a detailed account of such transmission and reflection conditions. Rather, we consider the limit where the sound speed inside the inclusion c_1 tends to infinity. In such a limit, which corresponds to non-penetrable inclusions, we verify that the energy is specularly reflected at the inclusion's boundary, which means that we have:

$$a_+^2(t, \mathbf{x}, \mathbf{k}) = a_+^2(t, \mathbf{x}, \mathbf{k} - 2\mathbf{k} \cdot \mathbf{n}(\mathbf{x})\mathbf{n}(\mathbf{x})), \quad \mathbf{x} \in \partial\Omega, \tag{16}$$

where $\mathbf{n}(\mathbf{x})$ is the outward unit normal to the boundary $\partial\Omega$ at $\mathbf{x} \in \partial\Omega$. In our comparison of various kinetic models in the next section, we shall restrict ourselves to these specific boundary conditions.

Cross-correlations in the presence of an inclusion. It remains to analyze the cross-correlation term $\mathcal{C}^\varepsilon(t, \mathbf{x})$. Although kinetic models have historically been applied to the derivation of energy densities as in [26], relatively straightforward generalizations, as they were developed e.g. in [4, 10], also allow us to derive kinetic models for correlations of wave fields propagating in possibly different media. The details of the computation are presented in Appendix A. The salient features of the derivation are that $W_\varepsilon^{12}(t, \mathbf{x}, \mathbf{k})$ converges as $\varepsilon \to 0$ to

$$W_0^{12}(t, \mathbf{x}, \mathbf{k}) = a_+^{12}(t, \mathbf{x}, \mathbf{k})\mathbf{b}_+^1(\mathbf{k})(\mathbf{b}_+^2(\mathbf{x}, \mathbf{k}))^* + a_-^{12}(t, \mathbf{x}, \mathbf{k})\mathbf{b}_-^1(\mathbf{k})(\mathbf{b}_-^2(\mathbf{x}, \mathbf{k}))^*,$$

where the propagating modes $a_\pm^{12}$ solve radiative transfer equations. More precisely, we find that a_+^{12} solves the equation

$$\begin{aligned}
&\frac{\partial a_+^{12}}{\partial t} + c_0\, \hat{\mathbf{k}} \cdot \nabla_\mathbf{x} a_+^{12} + \Sigma(\mathbf{k})\, a_+^{12} = Q(a_+^{12}), && \mathbf{x} \in \mathbb{R}^d \backslash \overline{\Omega}, \\
&a_+^{12}(t, \mathbf{x}, \mathbf{k}) = 0, && \mathbf{x} \in \partial\Omega, \ \mathbf{k} \cdot \mathbf{n}(\mathbf{x}) > 0,
\end{aligned} \tag{17}$$

with the initial conditions $a_+^{12}(0, \mathbf{x}, \mathbf{k}) = a_+^1(0, \mathbf{x}, \mathbf{k})$ for $\mathbf{x} \in \mathbb{R}^d \backslash \overline{\Omega}$ and $a_+^{12}(0, \mathbf{x}, \mathbf{k}) = 0$ for $\mathbf{x} \in \partial\Omega$. In other words, a_+^{12} solves the same radiative transfer equation as a_+^1 except that the solution vanishes inside Ω. Moreover, as in the case of energy densities, we have the relationship:

$$\lim_{\varepsilon \to 0} \mathcal{C}^\varepsilon(t, \mathbf{x}) = \int_{\mathbb{R}^d} a_+^{12}(t, \mathbf{x}, \mathbf{k}) d\mathbf{k}. \tag{18}$$

The physical interpretation of such a result is as follows. The two wave fields, one in the absence of an inclusion, and one in the presence of the inclusion, satisfy

different dispersion relations inside Ω because of the sound speed difference. As a consequence, they interfere destructively so that their interference pattern converges (weakly) to 0 inside Ω. Such destructive interferences may be explained as follows. Let us consider the two fields $p_\varepsilon^m(t, \mathbf{x}) = \chi(\mathbf{x})e^{\frac{i(c_m|\mathbf{k}_m|t + \mathbf{k}_m \cdot \mathbf{x})}{\varepsilon}}$ defined inside the inclusion for $m = 1, 2$ with different dispersion relations. We assume that the velocity fields vanish to simplify. Then, we verify by straightforward calculations that the Wigner transform $W_\varepsilon[p_\varepsilon^1, p_\varepsilon^2](t, \mathbf{x}, \mathbf{k})$ is given, up to lower order terms, by

$$e^{it\frac{c_1|\mathbf{k}_1| - c_2|\mathbf{k}_2|}{\varepsilon}} e^{i\frac{\mathbf{k}_1 - \mathbf{k}_2}{\varepsilon} \cdot \mathbf{x}} |\chi(\mathbf{x})|^2 \delta(\mathbf{k} - \frac{\mathbf{k}_1 + \mathbf{k}_2}{2}).$$

In the limit $\varepsilon \to 0$, the above term converges to 0 weakly (in the sense of distributions) unless $c_1|\mathbf{k}_1| = c_2|\mathbf{k}_2| = \omega$ and $\mathbf{k}_1 = \mathbf{k}_2$. This implies $c_1 = c_2$. Unless the latter constraint holds, the two wave fields p_ε^1 and p_ε^2 interfere destructively inside the inclusion. This is the reason why $a_+^{12} = 0$ inside Ω. We refer to the first part of the appendix for additional details.

Note that in the appendix, we make the additional assumption that the sound speed $\Delta c^2(\mathbf{x}) \equiv \Delta c^2(d(\mathbf{x}, \partial\Omega); \sqrt{\varepsilon})$ is regularized at the inclusion's interface. More specifically, we assume that it is a smooth function, which vanishes outside of Ω and is constant and equal to $c_1^2 - c_0^2$ at each point separated from the boundary $\partial\Omega$ by a distance at least equal to $\sqrt{\varepsilon}$. Such a smoothing of the interface allows us to derive a closed form equation for the Wigner transform of the two wave fields, which avoids the complications inherent to a jump in the sound speed and the related Snell-Descartes laws [5]. Since the resulting equations for a_+^{12} are independent of the regularization, we formally obtain that (17) also holds for sound speeds modeled by $c(\mathbf{x}) = c_0$ outside the inclusion and $c(\mathbf{x}) = c_1$ inside the inclusion. The appendix also covers configurations where inclusions have the same sound speed as the surrounding ($c_1 = c_0$) but where the fluctuations are suppressed ($\gamma = 1$; this could model a canopy gap in a forest), and the transition regime where the difference in the sound speeds Δc^2 is of the same order as the wavelength ε.

2.3 Diffusive regime

It is well known that solutions of radiative transfer equations in the small mean free path regime are well approximated by solutions to diffusion equations [15, 20]. Let us define the mean free path $l = c_0 \Sigma^{-1}$. The diffusive regime arises when $\eta = l/L \ll 1$, where L is the typical distance of wave propagation. Rescaling time and space as $t \to t/\eta^2$ and $\mathbf{x} \to \mathbf{x}/\eta$, we find in the limit $\eta \to 0$ that $a_\pm^1(t, \mathbf{x}, \mathbf{k})$ becomes independent of the angular variable $\hat{\mathbf{k}} = \mathbf{k}/|\mathbf{k}|$:

$$a_\pm^1(t, \mathbf{x}, \mathbf{k}) \approx U^1(t, \mathbf{x}, |\mathbf{k}|),$$

and more precisely that U^1 satisfies the following diffusion equation [15, 26]:

$$
\begin{aligned}
&\frac{\partial U^1}{\partial t} - D_0(|\mathbf{k}|)\Delta U^1 = 0, \qquad \mathbf{x} \in \mathbb{R}^3 \\
&U^1(0, \mathbf{x}, |\mathbf{k}|) = \frac{c_0}{4\pi|\mathbf{k}|^2} \int_{\mathbb{R}^3} a_\pm^1(0, \mathbf{x}, \mathbf{p})\delta(c_0(|\mathbf{k}| - |\mathbf{p}|))d\mathbf{p}.
\end{aligned}
\tag{19}
$$

The above equation is written in the three dimensional setting, $d = 3$, to simplify. The diffusion coefficient is defined as

$$D_0(|\mathbf{k}|) = \frac{c_0^2}{3[\Sigma(|\mathbf{k}|) - \lambda(|\mathbf{k}|)]},$$

(20)

where the anisotropy factor λ is given via the relation

$$\lambda(|\mathbf{k}|)\hat{\mathbf{k}} = \frac{c_0^2|\mathbf{k}|^2}{(4\pi)^2} \int_{\mathbb{R}^3} \hat{R}(\mathbf{p} - \mathbf{k})\hat{\mathbf{p}}\delta(c_0(|\mathbf{k}| - |\mathbf{p}|))d\mathbf{p}.$$

(21)

Similar expressions exist in two space dimensions [8].

The limiting equations for a_+^2 and a_+^{12} are obtained similarly in the limit $\eta \to 0$. We assume here that the inclusion Ω is perfectly reflecting ($c_1 = +\infty$) and is of size comparable to $L \gg \eta$. In the limit $\eta \to 0$, the specular reflection conditions (16) at the transport level translate into homogeneous Neumann boundary conditions for $U^2(t, \mathbf{x}, |\mathbf{k}|) \approx a_+^2(t, \mathbf{x}, \mathbf{k})$. Indeed, in the diffusion approximation, $a_+^2(t, \mathbf{x}, \mathbf{k}) = U^2(t, \mathbf{x}, |\mathbf{k}|) - \frac{\eta}{\Sigma(|\mathbf{k}|)}\mathbf{k} \cdot \nabla U^2$ [15, 20] up to lower-order terms in η. Multiplying the latter equation by $\mathbf{n}(\mathbf{x}) \cdot \mathbf{k}$ and integrating over the unit sphere $\hat{\mathbf{k}} = \frac{\mathbf{k}}{|\mathbf{k}|} \in S^{d-1}$ yields, using (16), that $\mathbf{n}(\mathbf{x}) \cdot \nabla U^2 = 0$ for $\mathbf{x} \in \partial\Omega$. So $U^2(t, \mathbf{x}, |\mathbf{k}|)$ solves (19) on $\mathbb{R}^3 \backslash \overline{\Omega}$ with the same initial conditions as before and satisfies

$$\frac{\partial U^2}{\partial \mathbf{n}} = 0, \qquad \mathbf{x} \in \partial\Omega.$$

(22)

Note that the above interface conditions at $\partial\Omega$ in the diffusive regime may be generalized to the case where the sound speed inside Ω is bounded ($c_1 < \infty$). Although this case is of practical interest, we do not consider it further here and refer the interested reader to [9] for more details.

Similarly, in the limit $\eta \to 0$, $U^{12}(t, \mathbf{x}, |\mathbf{k}|) \approx a_+^{12}(t, \mathbf{x}, \mathbf{k})$ still vanishes inside Ω so that $U^{12}(t, \mathbf{x}, |\mathbf{k}|)$ also solves (19) on $\mathbb{R}^3 \backslash \overline{\Omega}$ with the same initial conditions and verifies

$$U^{12} = 0, \qquad \mathbf{x} \in \partial\Omega.$$

(23)

To summarize, the energy density $U^1(t, \mathbf{x}, |\mathbf{k}|)$, which is equal to $\mathcal{E}(t, \mathbf{x})$ if the initial condition is concentrated at the frequency $\omega = c_0|\mathbf{k}|$, solves the unperturbed diffusion equation (19) in the absence of an inclusion. In the presence of the inclusion, $U^2(t, \mathbf{x}, |\mathbf{k}|)$ solves the same diffusion equation with Neumann boundary conditions at the boundary of the inclusion and $U^{12}(t, \mathbf{x}, |\mathbf{k}|)$ solves the same diffusion equation with vanishing boundary conditions on $\partial\Omega$.

3 Modeling and imaging of small volume inclusions

The macroscopic models derived in the preceding section lead us to the following observation. Provided that the random medium is sufficiently mixing -this will be addressed numerically in Section 5.1-, buried inclusions may be modeled by constitutive parameters in a transport equation or a diffusion equation. In the detection and the imaging of such inclusions, the microscopic inverse wave problem has thus been replaced by an

inverse transport problem or an inverse diffusion problem. The advantages of such a modification are the following: (i) we no longer need to model the random fluctuations explicitly and rather only need to estimate their statistical properties; (ii) the highly oscillatory wave fields (at a frequency of order ε^{-1}, whose accurate numerical description demands high computational costs) have been replaced by slowly varying phase-space energy densities (in the transport model) or physical energy densities (in the diffusive regime); (iii) the imaging of the inclusion depends on fewer macroscopic parameters such as the mean free path $c_0 \Sigma^{-1}$ in the transport regime and the diffusion coefficient D in the diffusive regime. The smaller these coefficients, the larger is the optical distance between the array of detectors and the inclusion and consequently the more difficult is the reconstruction of the detailed geometry of the inclusion. We refer the reader to e.g. [18, 23] and their references for more details on inverse transport and inverse diffusion theories.

In order to better assess the imaging capabilities of algorithms based on macroscopic energy densities and two-field correlations, we consider the case where the inclusions have *small volume*, in the sense that their properly defined diameter $2\mathsf{R}L$ is small compared to the typical distance of propagation L (i.e., $\mathsf{R} \ll 1$). The small volume approximation provides two benefits. The first benefit is that asymptotic expansions in the volume allow us to characterize the influence of the inclusion on the various kinetic quantities a_+^2, a_+^{12}, U^2 and U^{12} defined in the previous section. Such a characterization then enables us to compare the influence of the inclusion on the different types of available measurements. The second benefit is that the asymptotic influence typically depends on only a few geometric parameters of the inclusion such as its position and volume. Such simplified models can then be exploited in the imaging of the inclusion from available measurements; see e.g. [2, 3, 13].

3.1   Small volume inclusions in the transport regime

We first consider the influence of the inclusion on the transport regime quantities a_+^2 and a_+^{12}. We do not obtain explicit expressions for the quantities $a_+^1 - a_+^2$ and $a_+^1 - a_+^{12}$ in the full generality of transport equations. Rather we are interested in the order of magnitude of these quantities as a function of the volume of the inclusion. Let us recast the transport equation as

$$\frac{\partial a}{\partial t} + c_0 \hat{\mathbf{k}} \cdot \nabla_{\mathbf{x}} a + \Sigma a = \sigma_s K a, \tag{24}$$

where $a(0, \mathbf{x}, \mathbf{k})$ is prescribed, K is defined as Q in (12) with $\sigma(\mathbf{k}, \mathbf{p})$ replaced by $\sigma(\mathbf{k}, \mathbf{p})/\Sigma(\mathbf{k})$, and σ_s is a constant that would be defined as $\sigma_s = \Sigma$ in (11). We assume here that $|\mathbf{k}|$ is fixed and thus obtain a solution $a(t, \mathbf{x}, \hat{\mathbf{k}})$ function of the variables t, $\mathbf{x}$, $\hat{\mathbf{k}} = \mathbf{k}/|\mathbf{k}|$. We still denote momentum by $\mathbf{k}$. We choose initial conditions in the transport equation (24) of the form

$$a(0, \mathbf{x}, \mathbf{k}) = \delta(\mathbf{x}),$$

or more generally of the form $\delta(\mathbf{x})\phi(\hat{\mathbf{k}})$ with $\phi(\hat{\mathbf{k}})$ a smooth function. The smoothness of the latter function means that we do not know a priori in which direction to send the

energy in order to detect and image the inclusion. It can be verified that such initial conditions are indeed admissible as limits of Wigner transforms when $\varepsilon \to 0$ [8, 21].

In the limit where σ_s vanishes, the transport solution reads

$$a_0(t, \mathbf{x}, \mathbf{k}) = e^{-\Sigma t}\delta(\mathbf{x} - tc_0\hat{\mathbf{k}}).$$

This solution, which represents the (non-scattering) ballistic part, is independent of space dimension. Decomposing the exact solution to (24) as $a = a_0 + a_s$, we find that the scattered component solves the equation

$$\frac{\partial a_s}{\partial t} + c_0\hat{\mathbf{k}} \cdot \nabla_{\mathbf{x}}a_s + \Sigma a_s = \sigma_s K a_s + \sigma_s K a_0, \tag{25}$$

with vanishing initial conditions $a_s(0, \mathbf{x}, \mathbf{k}) = 0$. We have thus replaced the initial value problem by a non-homogeneous transport equation. Provided that scattering is of order $O(1)$ so that the ballistic part is not negligible, we obtain that a_s is of order comparable to the source term $\sigma_s K a_0$ from the well-posedness of the transport equation [15]. Note that we do not assume smallness of σ_s. We simply assume that it is not of the form σ_s/η for $\eta \ll 1$, for then we are in the diffusive regime of wave propagation, which is considered in Section 3.2.

In this context, let us analyze the influence of an inclusion on the quantities $a_+^1 - a_+^2$ and $a_+^1 - a_+^{12}$, which we re-label as $a - a^2$ and $a - a^{12}$. We define $a^2 = a_0^2 + a_s^2$ and $a^{12} = a_0^{12} + a_s^{12}$, where a_0^2 and a_0^{12} are the ballistic parts for energy and correlation measurements in the presence of the inclusion. Then we find that

$$a_0^{12}(t, \mathbf{x}, \mathbf{k}) = e^{-\Sigma t}\delta(\mathbf{x} - tc_0\hat{\mathbf{k}})\chi_{\text{inc}}(\mathbf{x}), \tag{26}$$

where $\chi_{\text{inc}}(\mathbf{x}) = 0$ when the segment $\{t\mathbf{x}, 0 < t < 1\}$ intersects Ω and $\chi_{\text{inc}}(\mathbf{x}) = 1$ otherwise. Similarly, we find that

$$a_0^2(t, \mathbf{x}, \mathbf{k}) = e^{-\Sigma t}\delta\big(\mathbf{x} - s(t, \mathbf{x}, \mathbf{k})c_0\hat{\mathbf{k}} - (t - s(t, \mathbf{x}, \mathbf{k}))c_0\hat{\mathbf{k}}'(t, \mathbf{x}, \mathbf{k})\big), \tag{27}$$

where $s(t, \mathbf{x}, \mathbf{k})$ is the time it takes for the signal to reach the inclusion Ω knowing that it will be at point $(\mathbf{x}, \mathbf{k})$ at time t (with $s = 0$ when such a scenario cannot happen), and where $\mathbf{k}'(t, \mathbf{x}, \mathbf{k})$ is the direction of the signal after scattering at $\partial\Omega$ (with $\mathbf{k}' = \mathbf{k}$ if no scattering has happened). We assume here that the inclusion is convex so that the ballistic part hits Ω at most once. Neglecting second-order interactions of the wave fields with the inclusion Ω (which is valid when Ω is sufficiently small), we obtain that the scattered parts a_s^2 and a_s^{12} satisfy the following equations

$$\frac{\partial a_s^\varphi}{\partial t} + c_0\hat{\mathbf{k}} \cdot \nabla_{\mathbf{x}}a_s^\varphi + \Sigma a_s^\varphi = \sigma_s K a_s^\varphi + \sigma_s K a_0^\varphi, \qquad \varphi = 2 \text{ or } \varphi = 12. \tag{28}$$

As a consequence, $a - a^2$ and $a - a^{12}$ are of the same order as their ballistic parts $a_0 - a_0^2$ and $a_0 - a_0^{12}$, respectively.

We obtain by inspection that both differences $a_0 - a_0^2$ and $a_0 - a_0^{12}$, integrated over momenta and over a spatial box of size L sufficiently large, are of order R^{d-1}, where we recall that $2\mathsf{R}L$ measures the physical diameter of the inclusion and d is space dimension. In other words, the inclusion modifies the intensities and correlations by an amount proportional to the solid angle of the inclusion seen from the source term location.

11

Assuming that the mean free path is not too small, so that multiple scattering does not dominate the transport solution, we therefore obtain that the influence of the inclusion on energy or correlation measurements (wherever the detectors may be located) is of order

$$\|a - a^2\|_{L^1} \approx \mathsf{R}^{d-1}, \qquad \|a - a^{12}\|_{L^1} \approx \mathsf{R}^{d-1}. \qquad (29)$$

Here the L^1 norm is in the space $(\mathbf{x}, \hat{\mathbf{k}}) \in \mathbb{R}^d \times S^{d-1}$.

Note however the following differences between $a - a^2$ and $a - a^{12}$. The former difference averages (in the phase space $(\mathbf{x}, \hat{\mathbf{k}})$) to 0 because specular reflection at $\partial\Omega$ conserves energy. Moreover a_0^2 allows us to detect the object no matter where the detectors are located. This is to be contrasted with the behavior of $a - a^{12}$. Note that $a - a^{12}$ has a positive average because some correlation is lost at the interface $\partial\Omega$ because of the mismatch of sound speeds inside and outside of the inclusion. Moreover, $a - a_0^{12}$ is non-zero only when detectors are located in the shadow of the inclusion viewed from the delta point source location. This means that in the absence of sufficient scattering, measuring the correlation a_0^{12} is not efficient and does not bring any additional information compared to the measurements of a_0^2. The situation is different in the diffusive regime as we now demonstrate.

3.2   Small volume inclusions in diffusion regime

Let us now consider the influence of localized small-volume inclusions on measurements in the regime of diffusion. We still assume that $|\mathbf{k}|$ is fixed and do not write it explicitly. The quantities a, a^2, and a^{12} are now replaced by U^1, U^2 and U^{12}, respectively. We refer to Section 2.3 for the equation they satisfy.

The influence of small volume inclusions in diffusive equations has been extensively studied recently; see [2, 13] and their references. Assuming that the inclusion is a ball of radius R to simplify (see the aforementioned references for extensions to more general geometries), we have shown in [7] that the perturbed energy density is given by

$$U^2(t, \mathbf{x}) = U^1(t, \mathbf{x}) + \frac{d}{d-1} D_0 \pi \mathsf{R}^d \int_0^t \nabla U^1(t - s, \mathbf{x}_b) \cdot \nabla G(s, \mathbf{x} - \mathbf{x}_b) ds + \mathcal{O}(\mathsf{R}^{d+1}), \quad (30)$$

where G is the Green function of the unperturbed diffusion equation (19). This expression holds for all space dimensions.

The behavior of the correlation difference $U^1 - U^{12}$ is quite different. We refer the reader to Appendix B for the details of the calculations. What the asymptotic analysis reveals is that:

$$U^{12}(t, \mathbf{x}) = U^{12}(t, \mathbf{x}) - D_0 \pi \mathsf{R}^{d-2} \int_0^t M(t - s) G(s, \mathbf{x}, \mathbf{x}_b) ds + \mathcal{O}(\mathsf{R}^{d-1}), \qquad (31)$$

where M is a coefficient explicitly defined in Appendix B, which is independent of the size of the inclusion. Here dimension $d \geq 3$. In dimension $d = 2$, the difference $U^1 - U^{12}$ is proportional to $|\log \mathsf{R}|$, whereas in dimension $d = 1$, the difference is of order $O(1)$. This shows that absorbing conditions like (23) have a much larger effect on measurements (at arbitrary positions $\mathbf{x}$) than Neumann conditions like (22).

12

4 Correlations and energy measurements: what is the best scenario?

How do the two types of measurements $\mathcal{E}_{\mathrm{inc}}^{\varepsilon}$ and $\mathcal{C}^{\varepsilon}(t,\mathbf{x})$ then compare in practice? We mention three possible scenarios and compare their advantages and disadvantages based on the results obtained in the preceding section on the influence of small volume inclusions.

(i) In the first scenario, we are only able to measure $\mathcal{E}_{\mathrm{inc}}^{\varepsilon}$. We do not have access to measurements in the *absence* of the inclusion and thus cannot form $\mathcal{E}_{\mathrm{inc}}^{\varepsilon} - \mathcal{E}^{\varepsilon}$, let alone $\mathcal{C}^{\varepsilon}(t,\mathbf{x}) - \mathcal{E}^{\varepsilon}$.

(ii) In the second scenario, we can estimate energy densities $\mathcal{E}^{\varepsilon}$ and $\mathcal{E}_{\mathrm{inc}}^{\varepsilon}$ and thus can form the difference $\mathcal{E}_{\mathrm{inc}}^{\varepsilon} - \mathcal{E}^{\varepsilon}$. We may not be able to measure wave fields accurately enough to form $\mathcal{C}^{\varepsilon}(t,\mathbf{x})$.

(iii) In the last scenario, we can measure $\mathbf{u}_{\varepsilon}^{\varphi}$ for $\varphi = 1, 2$ accurately and thus can form $\mathcal{E}^{\varepsilon}$, $\mathcal{E}_{\mathrm{inc}}^{\varepsilon}$, and $\mathcal{C}^{\varepsilon}(t,\mathbf{x})$ as well as the differences $\mathcal{E}_{\mathrm{inc}}^{\varepsilon} - \mathcal{E}^{\varepsilon}$ and $\mathcal{C}^{\varepsilon}(t,\mathbf{x}) - \mathcal{E}^{\varepsilon}$.

These scenarios are increasingly constraining technologically and practically. Imaging is hardest in the first scenario. The reason is that the measurements are inevitably noisy because the random wave energy density does not quite satisfy its deterministic limit at $\varepsilon = 0$. Because of this, the measured energy density is statistically stable (independent of the realization of the random medium) only up to a certain point. The influence of the inclusion, modeled by $a - a^2$ in the transport regime and by $U^1 - U^2$ in the diffusive regime, thus has to be larger than the noise level coming from our lack of knowledge of the specific realisation of the random medium. Detection and imaging of inclusions in highly heterogeneous random media with a given noise level has been addressed in [7] to which we refer the reader. We will provide numerical estimates of the noise level for specific random media in our section on numerical simulations.

Imaging is much simplified in scenarios (ii) and (iii) because we can form differential measurements: i.e., the difference of measurements in the absence and in the presence of the inclusion. Scenario (ii) requires energy measurements only, which ideally may be performed at a more macroscopic level than the wavelength, and are thus technologically less demanding than the measurements required in scenario (iii) to form accurate correlations.

Both scenarios (ii) and (iii) allow us to remove a substantial amount of noise coming from our lack of knowledge of the specific realization of the random medium. The reason is simple: path emanating from the source term and reaching the array of detectors without hitting the inclusion are not known exactly. They generate considerable noise in scenario (i). However, they cancel in scenarios (ii) and (iii) when we form the differences $\mathcal{E}_{\mathrm{inc}}^{\varepsilon} - \mathcal{E}^{\varepsilon}$ and $\mathcal{C}^{\varepsilon}(t,\mathbf{x}) - \mathcal{E}^{\varepsilon}$. In the latter two measurements, noise has to be proportional to the *product* of the size of the inclusion with our lack of knowledge of the random medium. Such a product is therefore quite small.

Now to the detailed comparison of scenarios (ii) and (iii). In the transport regime, we have observed that both differences $\mathcal{E}_{\mathrm{inc}}^{\varepsilon} - \mathcal{E}^{\varepsilon}$ and $\mathcal{C}^{\varepsilon}(t,\mathbf{x}) - \mathcal{E}^{\varepsilon}$ are roughly of order R^{d-1}, where $\mathsf{R} \ll 1$ is proportional to the diameter of the inclusion. Worse yet, the

correlation difference $\mathcal{C}^\varepsilon(t, \mathbf{x}) - \mathcal{E}^\varepsilon$ is not visible everywhere in the weak scattering limit. Scenario (ii) therefore provides the most adapted type of measurements for detection and imaging.

The situation is reversed in the diffusive regime. Because energy is conserved at the boundary of the inclusion in the case of specular reflection, the net effect of the inclusion's influence is a source term whose phase-space average vanishes. In the diffusive limit, this means a very localized effect of the inclusion so that its influence has to be obtained at a higher order (R^d versus R^{d-1}) in the inclusion's radius. In contrast, the vanishing boundary conditions (23) create a very strong constraint in the diffusive regime: because of increasing scattering, more and more paths reach the inclusion where they are absorbed. The net effect of the inclusion on measurements is an increase from a influence of order R^{d-1} in the transport regime to an influence of order $\mathsf{R}^{d-2} \gg \mathsf{R}^{d-1}$ in the diffusion regime.

When scattering is sizeable, correlations of the form $\mathcal{C}^\varepsilon(t, \mathbf{x})$ provide more signal to detect and image small volume inclusions than do energy measurements. Scenario (iii) becomes optimal among the three considered scenarios.

5   Validity of the transport model

This section concerns the numerical validation of the macroscopic radiative transfer model for the correlation $\mathcal{C}^\varepsilon(t, \mathbf{x})$. We pursue the research effort presented in [8] comparing wave simulations of $\mathcal{E}^\varepsilon(t, \mathbf{x})$ with transport theoretic predictions. After recalling the numerical tools that we use to solve wave and transport equations in Section 5.1, we show the very good accuracy of the radiative transfer model (17) to estimate $\mathcal{C}^\varepsilon(t, \mathbf{x})$ in Section 5.2. The statistical stability of the energy measurements $\mathcal{E}^\varepsilon(t, \mathbf{x})$ is briefly addressed in Section 5.3. A comparison of the influence of small inclusions on both $\mathcal{E}^\varepsilon(t, \mathbf{x})$ and $\mathcal{C}^\varepsilon(t, \mathbf{x})$, which provides direct information about what one can expect in terms of detection and imaging capabilities, is shown in Section 5.4. Explicit inversions are not considered here; see e.g. [7] where imaging of small-volume inclusions is considered.

5.1   Numerical setting

The numerical setting for wave propagation was described in detail in [8]. We recall here its main characteristics. The wave equation is solved in two-space dimensions as a mixed finite-difference discretization of the equations

$$\rho(\mathbf{x})\frac{\partial \mathbf{v}}{\partial t} + \nabla p = 0, \quad \kappa(\mathbf{x})\frac{\partial p}{\partial t} + \nabla \cdot \mathbf{v} = 0, \quad p(0, \mathbf{x}) = p_0(\mathbf{x}), \quad \mathbf{v}(0, \mathbf{x}) = \mathbf{v}_0(\mathbf{x}). \quad (32)$$

The computational domain is surrounded by a classical perfectly matched layer. We use a second order centered scheme for the discretization in time so that the overall scheme is second order both in time and space. The code is parallelized using the PETSc library, which allows for simulations on large domains. The initial condition is chosen so that only one frequency $|\mathbf{k}|$ is present at the transport level, at least approximately. More precisely, we choose:

$$\mathbf{u}_0(\mathbf{x}) = \left(\mathbf{0}, C_0 \exp\left(\frac{-|\mathbf{x} - \mathbf{x}_0|^2}{2\sigma^2} \right) J_0(|\mathbf{k}_0||\mathbf{x} - \mathbf{x}_0|) \right)^t = (\mathbf{0}, p_0)^t \quad (33)$$

where J_0 is the zero-th order Bessel function of the first kind. This initial condition exhibits an oscillatory behavior at the frequency $\mathbf{k}/\varepsilon$ (reduced frequency $\mathbf{k}$) and is localized in the vicinity of the point $\mathbf{x}_0$. The constant C_0 is chosen so that the energy associated to $\mathbf{u}_0$ is equal to one. The exponential term is chosen here to localize the source term. However, it has sufficiently slow variations in order not to interfere with the highly oscillatory Bessel function. Here, σ is chosen to be on the order of ten wavelengths so that the frequency content of $\mathbf{u}_0$ is primarily that of a single wavenumber $|\mathbf{k}_0|$.

In the simulations, we assume that

$$\rho_0 = 1, \quad \kappa(\mathbf{x}) = 1 + \sqrt{\varepsilon}\kappa_1\left(\frac{\mathbf{x}}{\varepsilon}\right), \tag{34}$$

where κ_1 is a stationary mean-zero random variable. The average sound speed is thus normalized to $c_0 = 1$. The fluctuations of the compressibility $\kappa_1(\mathbf{x})$ have been carefully modeled to satisfy prescribed power spectra in (7). This was done in the Fourier domain as in e.g. [8, 10].

The transport equations are solved by a Monte Carlo method as in [8]. The modified transport equation (17) is solved as usual, except that particles are killed when they hit $\partial\Omega$. The difference of intensities $a_+^1 - a_+^{12}$ is estimated by using the same variance reduction technique as in [8]: namely the random trajectories that do not hit $\partial\Omega$ are the same in the calculation of both a_+^1 and a_+^{12}. The initial condition at the transport level is

$$a_0(\mathbf{x}, \mathbf{k}) = \delta(\mathbf{x} - \mathbf{x}_0)\delta(|\mathbf{k}| - |\mathbf{k}_0|)|\mathbf{k}_0|^{-1}. \tag{35}$$

The power spectrum $\hat{R}$ is chosen isotropic and of the form

$$\hat{R}(r) = \begin{cases} \hat{R}_0 & \text{for} \quad r < M, \\ 0 & \text{for} \quad r > M, \end{cases}$$

where M is a given parameter such that $M > 2|\mathbf{k}_0|$. The scattering coefficient Σ is then given by

$$\Sigma(k) = \frac{k^3 \hat{R}_0}{4}. \tag{36}$$

In order to test the validity of the correlation prediction in the high scattering regime, where they are of interest, we have chosen a random medium with 8% of standard deviation, namely $\sqrt{R_0} = 8\%$ with R_0 given by $(2\pi)^2 R_0 = \pi M^2 \hat{R}_0$. We note that such high standard deviations for the heterogeneities in the random medium essentially preclude the use of scenario (i) in imaging unless the inclusion is quite large.

5.2 Accuracy of transport theoretic correlations

Accuracy of the transport model is tested following the same two steps we used in [8]. We first evaluate the transport parameter of the random medium, namely the mean free path $c_0 \Sigma^{-1}$ and then use this mean free path to assess the validity of the transport model to characterize the influence of a small-volume inclusions on the measurements.
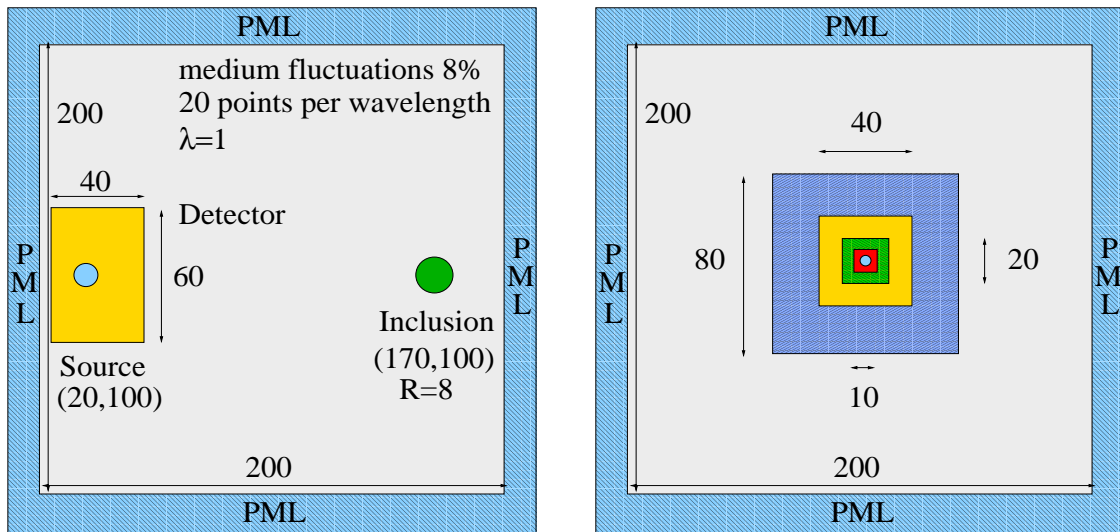
Figure 1: Domains of computation used in the numerical experiments.

Estimation of the transport parameters. Denoting by $\mathcal{D}$ the physical location of the array of detectors, we calculate numerically the following quantities

$$\mathcal{E}(t) = \int_{\mathcal{D}} \mathcal{E}(t, \mathbf{x}) d\mathbf{x} = \frac{1}{2} \int_{\mathcal{D}} \left(\kappa(\mathbf{x})(p^1(t, \mathbf{x}))^2 + \rho_0 |\mathbf{v}^1(t, \mathbf{x})|^2 \right) d\mathbf{x},$$

for the wave description and

$$\mathcal{A}^1(t) = \int_{\mathcal{D}} \int_{\mathbb{R}^2} a^1(t, \mathbf{x}, \mathbf{k}) d\mathbf{x} \, d\mathbf{k} = \int_{\mathcal{D}} \int_{S^1} a^1(t, \mathbf{x}, \hat{\mathbf{k}} | \mathbf{k}_0|) 2\pi |\mathbf{k}_0| d\mathbf{x} \, d\hat{\mathbf{k}},$$

for the transport prediction, where we dropped the subscript $+$ in a^1. Statistical stability for such wave measurements is of the order of $6 - 7\%$ based on numerical simulations on 4 realizations. We do not estimate the physical parameter Σ^{-1} based on a single realization as we did in [8] but rather average here over four realizations in order to obtain a more accurate description. The computational domain is of order 200×200 wavelengths and the detector array 60×40 wavelengths; see Fig.1 for the setting.

The transport energy density $\mathcal{A}^1 = \mathcal{A}^1[\Sigma]$ depends parametrically on Σ, whose theoretical prediction is given in (36). We minimize $\|\mathcal{E} - \mathcal{A}^1[\Sigma]\|_{L^2(0,T)}$ to estimate the mean free time Σ^{-1}. A value of $T = 1800$ yields a numerical estimate of $\Sigma_{\text{num}}^{-1} = 37$ while the theoretical value in (36) is given by $\Sigma_{\text{th}}^{-1} = 38.37$. The residual value of $\|\mathcal{E} - \mathcal{A}^1[\Sigma_{\text{num}}]\|_{L^2(0,T)} / \|\mathcal{A}^1[\Sigma_{\text{num}}]\|_{L^2(0,T)}$ is about 3.0%. Because fluctuations are here (purposely) significantly larger than what we had in [8] (8% versus 5%) and because the array of detectors is significantly smaller (60×40 wavelengths versus 150×150 wavelengths) there is considerably more noise in the estimation. Note however the good accuracy of the radiative transfer model since the best fit approximation lowers the residual value between wave energies and transport predictions to roughly 3%, a figure that would be quite accurate in many practical situations.

Validity of transport equations in the presence of an inclusion. We now add into the medium a spherical inclusion of radius R and effective sound speed twice as
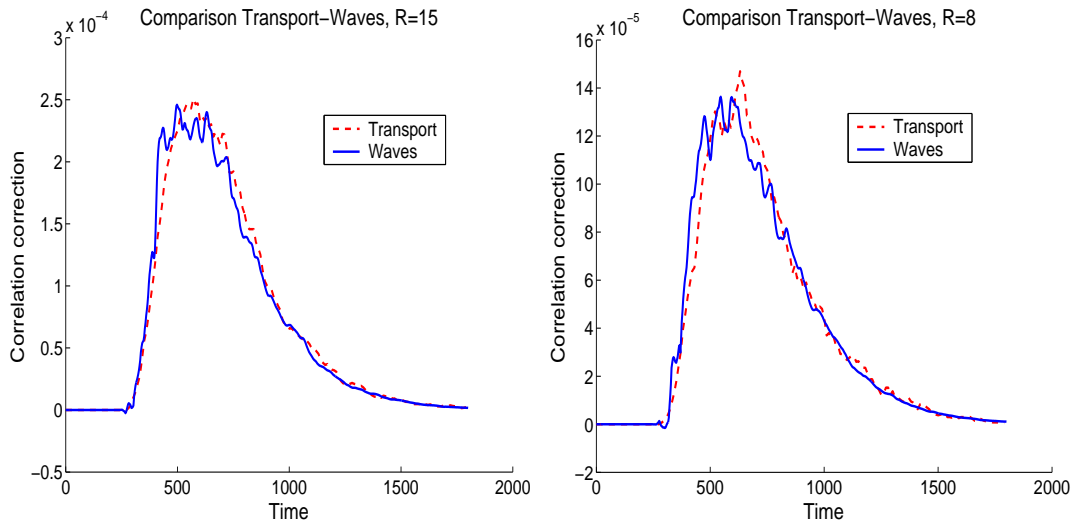
Figure 2: Verification of the accuracy of the modified transport regime: comparison wave in changing media - transport equations, for 8% fluctuations. We plot $\delta\mathcal{E}_{\mathrm{cor}}$ and $\delta\mathcal{A}_{\mathrm{cor}}$. The domain of computation is that of fig. 1. The $\mathsf{R} = 15$ (resp. $\mathsf{R} = 8$) case on the left (resp. right) is averaged over 2 (resp. 4) realizations.

large as the surrounding medium. The jump in the sound speed is regularized over two wavelength (2 times 20 grid points numerically). Fluctuations are suppressed inside the inclusion.

The influence on the correlations is denoted by $\delta\mathcal{E}_{\mathrm{cor}} = \mathcal{E} - \mathcal{C}$ for the wave fields and by $\delta\mathcal{A}_{\mathrm{cor}} = \mathcal{A}^1 - \mathcal{A}^{12}$ for the kinetic description, where

$$
\begin{aligned}
\mathcal{C}(t) &= \int_{\mathcal{D}} \mathcal{C}(t, \mathbf{x}) d\mathbf{x}, \\
&= \frac{1}{2} \int_{\mathcal{D}} \left(\kappa_1^{1/2} \kappa_2^{1/2}(\mathbf{x}) p^1(t, \mathbf{x}) \, p^2(t, \mathbf{x}) + \rho_0 \mathbf{v}^1(t, \mathbf{x}) \cdot \mathbf{v}^2(t, \mathbf{x}) \right) d\mathbf{x}, \\
\mathcal{A}^{12}(t) &= \int_{\mathcal{D}} \int_{\mathbb{R}^2} a^{12}(t, \mathbf{x}, \mathbf{k}) d\mathbf{x} \, d\mathbf{k} = \int_{\mathcal{D}} \int_{S^1} a^{12}(t, \mathbf{x}, \hat{\mathbf{k}}|\mathbf{k}_0|) 2\pi |\mathbf{k}_0| d\mathbf{x} \, d\hat{\mathbf{k}}.
\end{aligned}
$$

Numerical comparisons of $\delta\mathcal{E}_{\mathrm{cor}}$ and $\delta\mathcal{A}_{\mathrm{cor}}$ are presented in Fig.2 for balls of radius $\mathsf{R} = 15$ (left) and $\mathsf{R} = 8$ (right) wavelengths, respectively. The calculations are averaged over 2 realizations in the case $\mathsf{R} = 15$ and over 4 realizations in the case $\mathsf{R} = 8$ to slightly suppress oscillations (smoothing in time would have a similar effect). We observe a very good agreement between the wave simulations and the kinetic predictions. Note moreover that both $\delta\mathcal{E}_{\mathrm{cor}} \geq 0$ and $\delta\mathcal{A}_{\mathrm{cor}} \geq 0$ as is expected physically since correlation is lost at the inclusion's location because of the mismatch in the sound speed.

5.3 Statistical stability

Statistical stability of the energy measurements is a crucial component for detection and imaging in the framework of scenario (i). As we have already said, lack of knowledge of the realization of the random medium translates into a significant noise level between the true energy density $\mathcal{E}$ and its kinetic prediction. Detection and imaging are then

possible only when the influence of the inclusion is larger than this noise level [7], unless the inclusion possesses a particular statistical signature that is very different from that of the random medium, an extremely unlikely scenario in wave propagation in highly heterogeneous media.

How unstable measurements of $\mathcal{E}$ are primarily depends on two parameters: the level of disorder R_0 and the size of the detector $\mathcal{D}$. Consider the relative standard deviation

$$S(t) = \frac{\sigma[\mathcal{E}](t)}{\mathbb{E}[\mathcal{E}](t)},$$

where σ denotes standard deviation, $\mathbb{E}$ average (mathematical expectation) and $\mathcal{E}$ the energy averaged over the array of detectors. The average and the standard deviation are computed over 8 realizations of the random medium and the measurements are performed over an array of size 40×60 centered at the point $(100, 100)$. Fig.3 (left panel) shows the relative standard deviation $S(t)$ in that configuration. We do not possess theoretical models for $S(t)$. The growth observed in Fig.3 may be explained as follows. It is known in the homogenization of rapidly varying ordinary differential equations that, in the appropriate context, the solution converges to a deterministic solution (following the law of large numbers), and the next-order corrector becomes a stochastic integral (following a generalization of the central limit theorem). The variance of such a stochastic integral increases with time (it starts at 0 at time $T = 0$ as in Fig.3) before it stabilizes in a way depending on the nature of the problem at hand. A similar process is observed here. A more careful explanation requires a theoretical model for the correction term $\mathcal{E}^\varepsilon - \mathcal{E}^0$, where $\mathcal{E}^0(\mathbf{x}) = \int_{\mathbb{R}^d} a_+^1(\mathbf{x}, \mathbf{k}) d\mathbf{k}$ with the notation used in earlier sections. Such a model does not exist at present.
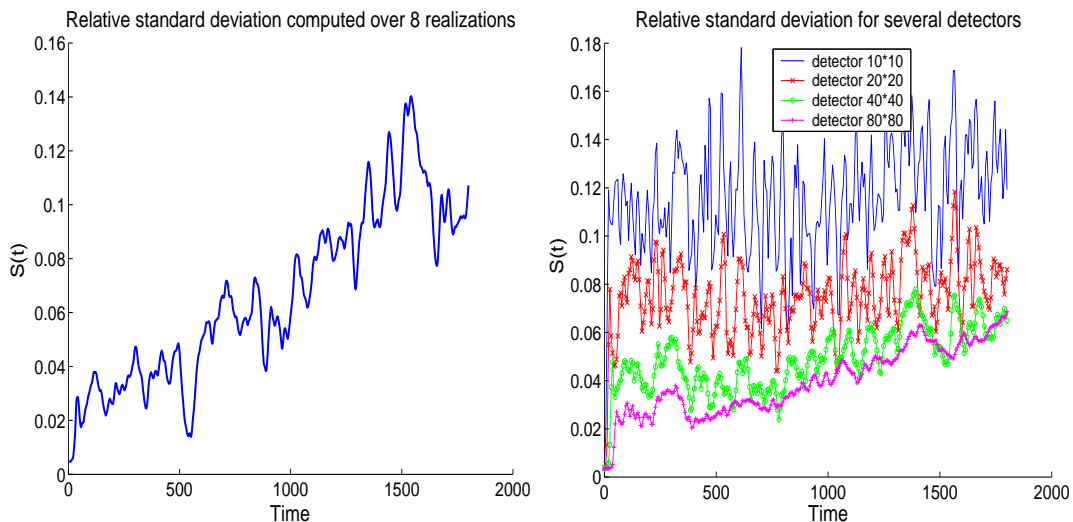

Figure 3: Left: $S(t)$ performed over 8 realizations, for a 40×60 detector located at the center of the domain. Right: $S(t)$ performed over 20 realizations and computed for 4 different detectors located at the center.

The right panel of Fig.3 shows the evolution of $S(t)$ for four different detectors D_k, $0 \leq k \leq 3$ centered in the middle of the domain and of sizes equal to 10×10, 20×20, 40×40, and 80×80, respectively, based on 20 realizations of the random medium. See

18

Fig.1 (right) for the computational setup. Averages of the statistical instability in time are defined by

$$I_k = \frac{1}{500} \int_{1000}^{1500} S_k(t)dt, \qquad 0 \le k \le 3,$$

for $S_k(t)$ measured on D_k. We obtain the results $I_0 = 0.124$, $I_1 = 0.080$, $I_2 = 0.059$, and $I_3 = 0.051$, respectively. We conclude that larger detector sizes provide more stable measurements, as we expected, but that the convergence of I_k to 0 as k increases is quite slow, and certainly slower than what would be predicted by the law of large numbers for uncorrelated random variables. Such a behavior has to be explained by long-range spatial correlations of the corrector $\mathcal{E}^\varepsilon - \mathcal{E}^0$. To further quantify this long-range correlation, we consider the following four random variables $E_k(t)$ for $0 \le k \le 3$, where $E_0(t)$ is the energy detected on the detector D_0 and where $E_k(t)$, $1 \le k \le 3$ is the difference of the energies measured on D_k and on D_{k-1} (i.e. on a ring we call G_k). The expected values of the $E_k(t)$ are given in Fig.4 (left). Their correlation matrix is given by

$$C_{ij}(t) = \frac{\mathbb{E}\{(E_i(t) - \mathbb{E}\{E_i(t)\})(E_j(t) - \mathbb{E}\{E_j(t)\})\}}{\sigma[E_i(t)]\sigma[E_j(t)]}.$$

The values of $C_{0k}(t)$ for $k = 1, 2, 3$ are plotted in Fig.4 (right). Let us denote by $\bar{C}_{ij}$ the
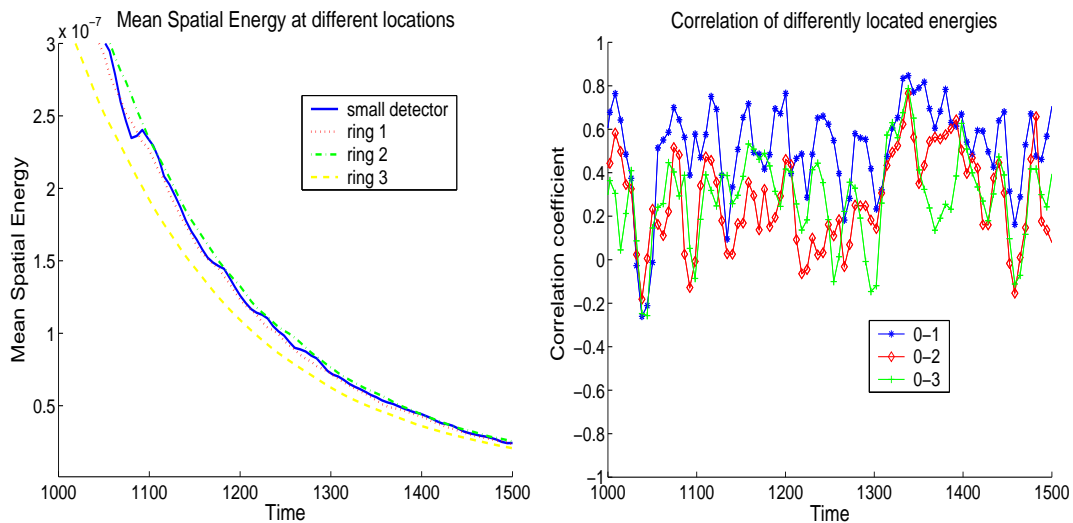

Figure 4: Left: Averaged energies over D_0 and the rings G_k, $k = 1, 2, 3$. Right: Correlations C_{0k} for $k = 1, 2, 3$.

average of $C_{ij}(t)$ over the interval $[1000, 1500]$. We find the following values: $\bar{C}_{01} = 0.54$, $\bar{C}_{02} = 0.29$, $\bar{C}_{03} = 0.32$, $\bar{C}_{12} = 0.96$, $\bar{C}_{13} = 0.46$, and $\bar{C}_{23} = 0.73$. The random variables become thus less correlated as their spatial domains of integration separate, but we still observe a very strong long-range correlation between the energies measured on the disjoint rings G_k. This is not good news for imaging as it indicates that the corrector $\mathcal{E}^\varepsilon - \mathcal{E}^0$ is random (i.e., strongly depends on the realization of the random medium) and has such a long correlation length that its effect can barely be mitigated by increasing the size of the array of measurements. Such long range correlations are characteristics of the regime of wave localization; see [27, 28].

5.4 Influence on detection and imaging

Let us come back to a comparison of the detection and imaging capabilities in the scenarios presented in Section 4. We define $\delta\mathcal{E}_{\text{inc}} = \mathcal{E} - \mathcal{E}_{\text{inc}}$ where

$$\mathcal{E}_{\text{inc}}(t) = \int_{\mathcal{D}} \mathcal{E}_{\text{inc}}(t, \mathbf{x}) d\mathbf{x},$$

$$= \frac{1}{2} \int_{\mathcal{D}} \left(\kappa_2(\mathbf{x})(p^2(t, \mathbf{x}))^2 + \rho_0(\mathbf{x})|\mathbf{v}^2(t, \mathbf{x})|^2 \right) d\mathbf{x}.$$

Thus $\delta\mathcal{E}_{\text{cor}}$ is the correlation correction while $\delta\mathcal{E}_{\text{inc}}$ is the correction introduced by the inclusion on the energy. We show in Fig.5 the evolution of $\delta\mathcal{E}_{\text{cor}}$ and $\delta\mathcal{E}_{\text{inc}}$ (normalized by $\mathcal{E}(0)$) in the case of 8% of fluctuations in the random medium and for three different sizes of the inclusion: $R = 4$, $R = 8$ and $R = 15$. The energies and correlations associated to the cases $R = 4$ and $R = 8$ are averaged over 4 realizations while they are averaged over 2 realizations in the case $R = 15$. In all cases, the correlation correction is significantly
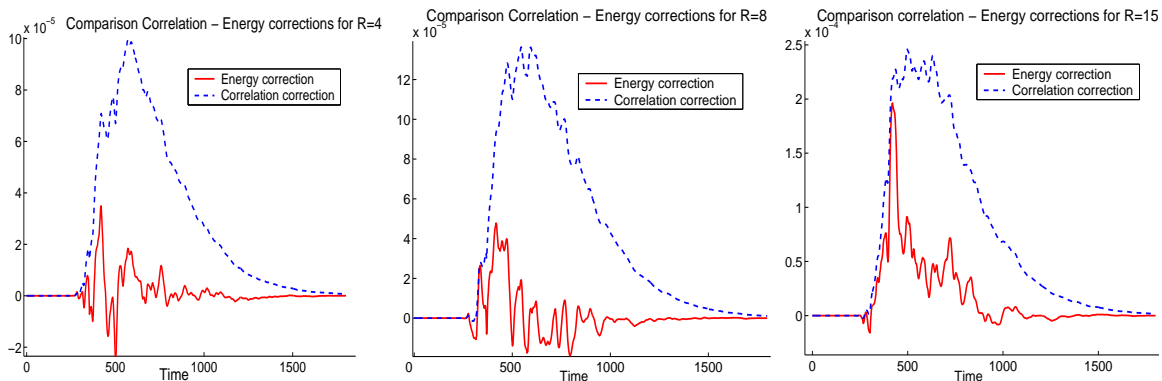

Figure 5: Comparison correlation correction - energy correction, for 8% fluctuations, for the radii $R = 4$, $R = 8$ and $R = 15$, respectively. The case $R = 15$ is averaged over 2 realizations while the cases $R = 8$ and $R = 4$ are averaged over 4 realizations.

larger than the energy correction. This is compatible with our analysis of small volume corrections in the diffusive regime, where scattering is quite important.

The same quantities as in Fig.5 are reproduced in Fig.6 when the fluctuations in the random medium have a standard deviation equal to 3% instead of 8%. The energy variations are now comparable to or even larger than the correlation variations, in agreement with our theoretical predictions in the transport regime. In such a configuration, scenario (iii) is not necessarily optimal and should not perform better than scenario (ii). Of course, a combination of both energy and correlation measurements can only improve imaging.

Finally, we plot on the same graph the relative correlation correction $\delta\mathcal{E}_{\text{cor}}(t)/\mathcal{E}(t)$, the relative energy correction $\delta\mathcal{E}_{\text{inc}}(t)/\mathcal{E}(t)$ and the relative standard deviation $S(t)$, for two size of the inclusion $R = 8$ and $R = 15$ in Fig.7. In the case $R = 8$, the statistical error between the wave energy and the transport prediction are so overwhelming that noise is significantly larger than the inclusion's influence on energy measurements. The situation slightly improves when $R = 15$. Energy measurements are however still quite small compared to the noise level so that detection capabilities remain small; see [7] for a
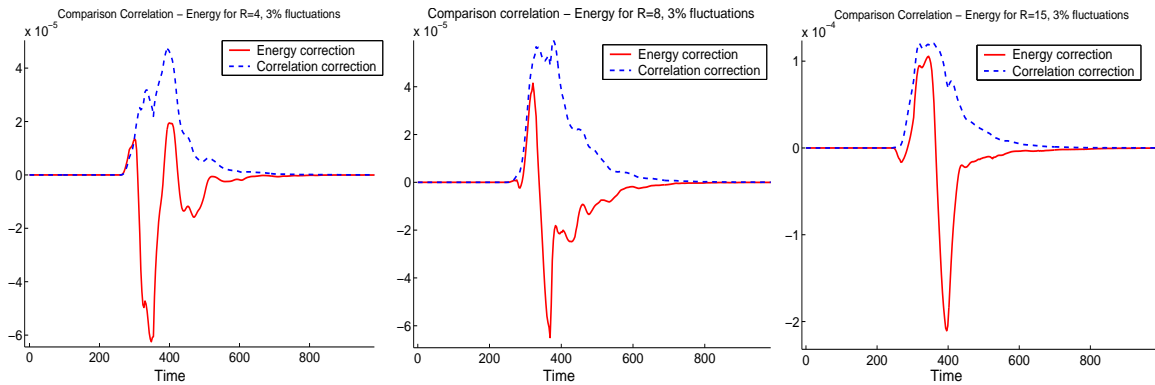
Figure 6: Comparison correlation correction - energy correction, for 3% fluctuations, for radii equal to $R = 4$, $R = 8$ and $R = 15$. The ballistic part of the waves is significant.
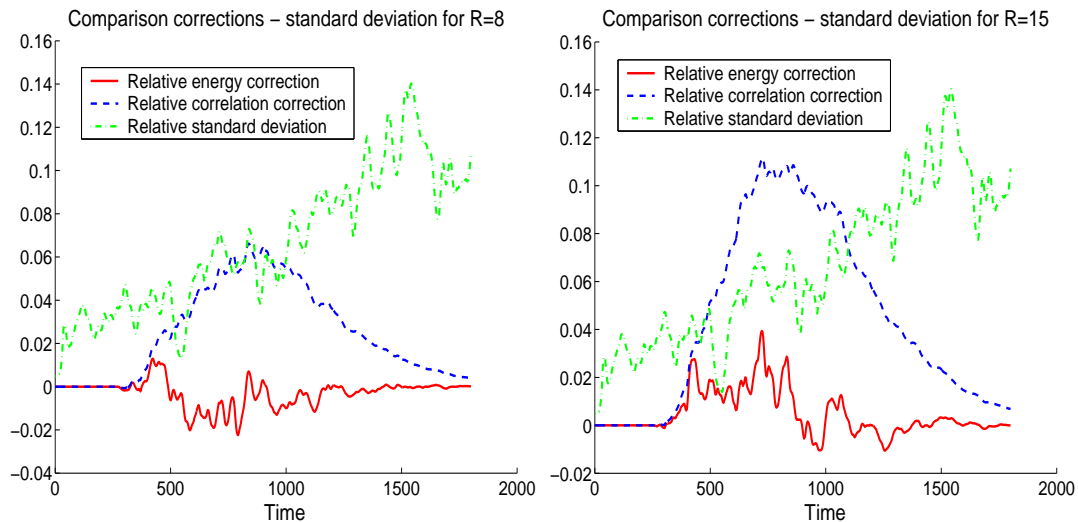

Figure 7: Comparison relative standard deviation - relative correlation correction - relative energy correction, for 8% fluctuations and $R = 8$ (left) and $R = 15$ (right).

description of standard statistical test that can be used in such a detection. Scenario (i) will thus fail to provide good detection and imaging results in such random environments.

Scenarios (ii) and (iii) provide better configurations. Because we now are in a position to obtain differential measurements, the noise generated by our lack of knowledge of the random medium is significantly reduced. Note however that the difference of energies is on the order of 1% of the total energy when $R = 8$ and on the order of 2% when $R = 15$. Thus, in the presence of external noise that is independent of the random medium, e.g. generated by external sources or by defects in the measurements, scenario (ii) may provide limited detection and imaging capabilities. The influence of the inclusion on the correlation is significantly higher, on the order of 6% of total energy when $R = 8$ and on the order of 10% when $R = 15$. When accurate measurements can be obtained in scenario (iii), which requires that one sample the wave fields at the level of the wavelength to capture correlations accurately, they provide the most accurate data towards the detection and imaging of inclusions buried in a random medium.

6 Conclusions

The two main contributions of the paper are (i) the numerical validation of radiative transfer equations to model the energy density and the two-field correlations of waves propagating in highly heterogeneous media; and (ii) the characterization of small-volume inclusions for imaging based on the three scenarios considered in Section 4 in the radiative transfer and in the diffusive regimes of wave propagation. Inclusions here were modeled by changes in the average wave speed and/or changes in the statistics of the random fluctuations.

We have shown that differential measurements were necessary when the influence of the inclusion was larger than the statistical instability resulting from our lack of knowledge of the underlying random medium. We have shown that wave-field correlations provided superior imaging capabilities in highly scattering environment. In the regime of moderate scattering however, wave field correlations do not provide any additional advantage compared to energy density differential measurements.

In the absence of differential measurements, imaging based on scenario (i) remains the only choice. We have shown in Section 5 how large the statistical instability may become in random media with large fluctuations (see Fig.3). Further theoretical studies are necessary to quantify this instability and understand its spatial and temporal behavior (such as the increase observed for short times in Fig.3 and the spatial long range correlations which explain why the instability barely decreases as the size of the detectors increases).

Acknoledgments

A   Derivation of the transport equations

We derive in this appendix the high-frequency asymptotics for the two-field correlation $W_\varepsilon^{1,2}$. Recall that each field $\mathbf{u}_\varepsilon^\varphi$ is a solution of

$$\varepsilon \frac{\partial \mathbf{u}_\varepsilon^\varphi}{\partial t} + A_\varepsilon^\varphi \mathbf{u}_\varepsilon^\varphi = 0, \qquad \varphi = 1, 2, \qquad t > 0, \qquad \mathbf{x} \in \mathbb{R}^d, \tag{37}$$

with appropriate initial conditions. We assume that A_ε^φ has the following form

$$A_\varepsilon^\varphi = - \begin{pmatrix} 0 & c_0^2 \\ \varepsilon^2 \Delta & 0 \end{pmatrix} + V_\varepsilon^\varphi(\mathbf{x}, \frac{\mathbf{x}}{\varepsilon}) K, \qquad K = \begin{pmatrix} 0 & 1 \\ 0 & 0 \end{pmatrix}, \qquad \mathbf{x} \in \mathbb{R}^d. \tag{38}$$

Here, c_0 is the average speed of propagation and the potentials V_ε^φ are given by

$$V_\varepsilon^1(\mathbf{x}, \frac{\mathbf{x}}{\varepsilon}) = \sqrt{\varepsilon} V(\frac{\mathbf{x}}{\varepsilon}), \qquad V_\varepsilon^2(\mathbf{x}, \frac{\mathbf{x}}{\varepsilon}) = -\chi(\mathbf{x}) \Delta c^2 + \sqrt{\varepsilon}(1 - \gamma \chi(\mathbf{x})) V(\frac{\mathbf{x}}{\varepsilon}), \tag{39}$$

where V accounts for the random fluctuations and is a mean-zero stationary process, and Δc^2 is the velocity jump at the inclusion's boundary. As in (8), γ is a parameter modeling

22

fluctuations within the inclusion, with $\gamma = 1$ if random fluctuations are suppressed, and $\gamma = 0$ is they are still present and have the same statistics as outside of Ω. For simplicity, we assume that the inclusion is spherical and denote by χ its characteristic function, namely $\chi(\mathbf{x}) = 1$ when $\mathbf{x} \in B(\mathbf{x}_0, \mathsf{R})$ and $\chi(\mathbf{x}) = 0$ otherwise. We regularize the jump of the velocity and replace χ by a smooth cut-off function χ^δ such that

$$\chi^\delta \in \mathcal{C}_0^\infty(\mathbb{R}^d), \quad 0 \leq \chi^\delta \leq 1, \quad \chi^\delta(\mathbf{x}) = \begin{cases} 1 & \text{if} \quad \mathbf{x} \in B(\mathbf{x}_0, \mathsf{R} - \delta), \\ 0 & \text{if} \quad \mathbf{x} \notin B(\mathbf{x}_0, \mathsf{R}). \end{cases} \tag{40}$$

Such a function can be obtained by convolution of a standard mollifier $\left(\frac{\delta}{2}\right)^{-d} \psi\left(\frac{2\mathbf{x}}{\delta}\right)$ of unit integral with the characteristic function of the ball $B(x_0, \mathsf{R} - \delta/2)$. Then χ^δ verifies the property

$$\sup_{\mathbf{x} \in \mathbb{R}^d} |\nabla_{\mathbf{x}}^{(p)} \chi^\delta(\mathbf{x})| \leq \frac{C_p}{\delta^p}, \tag{41}$$

where C_p is a constant independent of δ, chosen such that $0 < \varepsilon \ll \delta(\varepsilon) \ll 1$, and for concreteness chosen as $\delta(\varepsilon) = \sqrt{\varepsilon}$.

The Wigner function of the two fields is defined as

$$W_\varepsilon^{1,2}(t, \mathbf{x}, \mathbf{k}) := W_\varepsilon(t, \mathbf{x}, \mathbf{k}) = \int_{\mathbb{R}^d} e^{i\mathbf{k}\cdot\mathbf{y}} \, \mathbf{u}_\varepsilon^1(t, \mathbf{x} - \frac{\varepsilon\mathbf{y}}{2}) \left(\mathbf{u}_\varepsilon^2\right)^* (t, \mathbf{x} + \frac{\varepsilon\mathbf{y}}{2}) \frac{d\mathbf{y}}{(2\pi)^d},$$

and solves

$$\varepsilon \frac{\partial W_\varepsilon}{\partial t} + W\left[A_\varepsilon^1 \mathbf{u}_\varepsilon^1, \mathbf{u}_\varepsilon^2\right] + W\left[\mathbf{u}_\varepsilon^1, A_\varepsilon^2 \mathbf{u}_\varepsilon^2\right] = 0.$$

Note that only the second field $\mathbf{u}_\varepsilon^2$ depends on the regularization parameter δ.

Asymptotic expansions. We introduce the two-scale version of W_ε

$$W_\varepsilon(t, \mathbf{x}, \mathbf{k}) = W_\varepsilon(t, \mathbf{x}, \frac{\mathbf{x}}{\varepsilon}, \mathbf{k}),$$

and with $\mathbf{y} = \varepsilon^{-1}\mathbf{x}$, the expansion

$$W_\varepsilon(t, \mathbf{x}, \mathbf{y}, \mathbf{k}) = W^0(t, \mathbf{x}, \mathbf{k}) + \sqrt{\varepsilon} W^1(t, \mathbf{x}, \mathbf{y}, \mathbf{k}) + \varepsilon W^2(t, \mathbf{x}, \mathbf{y}, \mathbf{k}). \tag{42}$$

We start with the term $W\left[\mathbf{u}_\varepsilon^1, A_\varepsilon^2 \mathbf{u}_\varepsilon^2\right]$ involving the potentials V_ε^2. Thanks to (39), $W\left[\mathbf{u}_\varepsilon^1, V_\varepsilon^2 K \mathbf{u}_\varepsilon^2\right]$ can be written as

$$W\left[\mathbf{u}_\varepsilon^1, V_\varepsilon^2 K \mathbf{u}_\varepsilon^2\right] = -\Delta c^2 W\left[\mathbf{u}_\varepsilon^1, \chi^\delta \mathbf{u}_\varepsilon^2\right] K^* + \sqrt{\varepsilon} W\left[\mathbf{u}_\varepsilon^1, (1 - \gamma\chi^\delta)V \mathbf{u}_\varepsilon^2\right] K^*,$$

and $\chi^\delta(\mathbf{x} + \varepsilon\mathbf{y}/2)$ can be expanded as

$$\chi^\delta(\mathbf{x} + \varepsilon\mathbf{y}/2) = \chi^\delta(\mathbf{x}) + \frac{\varepsilon}{2} \mathbf{y} \cdot \nabla_{\mathbf{x}} \chi^\delta(\mathbf{x}) + r^\varepsilon(\mathbf{x}, \mathbf{y}),$$

where R^ε is a function such that $|r^\varepsilon(\mathbf{x}, \mathbf{y})| \leq C\frac{\varepsilon^2}{\delta^2}$ for every $\mathbf{y}$ in a bounded set and whose support in $\mathbf{x}$ is of order $\mathcal{O}(\delta)$: $\text{Meas}(\text{supp}_{\mathbf{x} \in \mathbb{R}^d} r^\varepsilon(\mathbf{x}, \mathbf{y})) \leq C\delta(\varepsilon)$ for $\mathbf{y}$ bounded. Owing to the fact that

$$W\left[\mathbf{u}_\varepsilon^1, \mathbf{y}\, \mathbf{u}_\varepsilon^2\right] = \frac{1}{(2\pi)^d} \int_{\mathbb{R}^d} e^{i\mathbf{k}\cdot\mathbf{y}} \, \mathbf{y}\, \mathbf{u}_\varepsilon^1(\mathbf{x} - \frac{\varepsilon\mathbf{y}}{2}) \left(\mathbf{u}_\varepsilon^2\right)^*(\mathbf{x} + \frac{\varepsilon\mathbf{y}}{2})\, d\mathbf{y} = \frac{1}{i} \nabla_{\mathbf{k}} W_{\varepsilon,\delta}(\mathbf{x}, \mathbf{k}),$$

23

we expand $W\left[\mathbf{u}_\varepsilon^1, V_\varepsilon^2 K \mathbf{u}_\varepsilon^2\right]$ as follows. Let $\varphi(\mathbf{x}, \mathbf{k})$ be a test function such that its Fourier transform with respect to the second variable $\hat{\varphi}(\mathbf{x}, \mathbf{y})$ is compactly supported and of class $\mathcal{C}_0^\infty(\mathbb{R}^{2d})$. Denote by $W^{i,j}$, $i = 1, 2$, $j = 1, 2$ the entries of the matrix $W\left[\mathbf{u}_\varepsilon^1, V_\varepsilon^2 K \mathbf{u}_\varepsilon^2\right]$ and by $W_\varepsilon^{i,j}$ that of W_ε. Then, for W_ε regular enough, we have

$$-\Delta c^2 \langle W^{i,j}\left[\mathbf{u}_\varepsilon^1, \chi^\delta \mathbf{u}_{\varepsilon,\delta}^2\right], \varphi\rangle = \langle A^\varepsilon W_\varepsilon^{i,j}, \varphi\rangle + \varepsilon\langle B^\varepsilon W_\varepsilon^{i,j}, \varphi\rangle + \mathcal{O}(\varepsilon^{3/2}),$$

where $A^\varepsilon = -\Delta c^2 \chi^\delta$ and B^ε is the operator $-\frac{1}{2i}\Delta c^2 \nabla_\mathbf{x}\chi^\delta \cdot \nabla_\mathbf{k}$. The error of order $\varepsilon^{3/2}$ is obtained after the following computation:

$$
\begin{aligned}
&\langle W^{i,j}\left[\mathbf{u}_\varepsilon^1, r^\varepsilon\,\mathbf{u}_\varepsilon^2\right], \varphi\rangle \\
=\quad & \frac{1}{(2\pi)^d}\int_{\mathbb{R}^d}\int_{\mathbb{R}^d}\int_{\mathbb{R}^d} e^{i\mathbf{k}\cdot\mathbf{y}} r^\varepsilon(\mathbf{x}, \mathbf{y})\mathbf{u}_\varepsilon^1(\mathbf{x} - \frac{\varepsilon\mathbf{y}}{2})\,(\mathbf{u}_\varepsilon^2)^*(\mathbf{x} + \frac{\varepsilon\mathbf{y}}{2})\,\varphi(\mathbf{x}, \mathbf{k})d\mathbf{x}d\mathbf{y}d\mathbf{k}, \\
=\quad & \int_{\mathbb{R}^d}\int_{\mathbb{R}^d} r^\varepsilon(\mathbf{x}, \mathbf{y})\mathbf{u}_\varepsilon^1(\mathbf{x} - \frac{\varepsilon\mathbf{y}}{2})\,(\mathbf{u}_\varepsilon^2)^*(\mathbf{x} + \frac{\varepsilon\mathbf{y}}{2})\,\hat{\varphi}(\mathbf{x}, \mathbf{y})d\mathbf{x}d\mathbf{y}, \\
\leq\quad & C\frac{\varepsilon^2}{\delta^2}\int_{\text{supp}_\mathbf{x} R}\int_{\text{supp}_\mathbf{y}\varphi}\mathbf{u}_\varepsilon^1(\mathbf{x} - \frac{\varepsilon\mathbf{y}}{2})\,(\mathbf{u}_\varepsilon^2)^*(\mathbf{x} + \frac{\varepsilon\mathbf{y}}{2})\,\sup_\mathbf{x}|\hat{\varphi}(\mathbf{x}, \mathbf{y})|d\mathbf{x}d\mathbf{y}, \\
\leq\quad & C\frac{\varepsilon^2}{\delta^2}\|\mathbf{u}_\varepsilon^1\|_{L^2(C^\delta)}\|\mathbf{u}_\varepsilon^2\|_{L^2(C^\delta)},
\end{aligned}
$$

where C^δ are sets of measure of order $\delta = \sqrt{\varepsilon}$. Thus, if $\mathbf{u}_\varepsilon^1$ and $\mathbf{u}_\varepsilon^2$ are smooth enough so that $\|\mathbf{u}_\varepsilon^\varphi\|_{L^2(C^\delta)} = \mathcal{O}(\sqrt{\delta})$, we obtain an error of order $\varepsilon^{3/2}$.

In the same way,

$$
\begin{aligned}
\langle W^{i,j}\left[\mathbf{u}_\varepsilon^1, (1 - \gamma\chi^\delta(\cdot))V(\tfrac{\cdot}{\varepsilon}), \mathbf{u}_\varepsilon^2\right], \varphi\rangle &= \langle W^{i,j}\left[\mathbf{u}_\varepsilon^1, V(\tfrac{\cdot}{\varepsilon}), \mathbf{u}_\varepsilon^2\right], (1 - \gamma\chi^\delta)\varphi\rangle + \mathcal{O}(\varepsilon), \\
&= \int_{\mathbb{R}^{3d}} e^{i\frac{\mathbf{x}\cdot\mathbf{p}}{\varepsilon}}(1 - \gamma\chi^\delta(\mathbf{x}))\hat{V}(\mathbf{p})\,W_\varepsilon^{i,j}(\mathbf{x}, \mathbf{k} - \mathbf{p})\,\varphi(\mathbf{x}, \mathbf{k})\frac{d\mathbf{x}d\mathbf{k}d\mathbf{p}}{(2\pi)^d} + \mathcal{O}(\varepsilon), \\
&= \langle(1 - \gamma\chi^\delta)\mathcal{K}_\varepsilon W_\varepsilon^{i,j}, \varphi\rangle + \mathcal{O}(\varepsilon),
\end{aligned}
$$

where

$$(\mathcal{K}_\varepsilon W)(\mathbf{x}, \mathbf{k}) = \int_{\mathbb{R}^d} e^{i\frac{\mathbf{x}\cdot\mathbf{p}}{\varepsilon}}\,\hat{V}(\mathbf{p})\,W(\mathbf{x}, \mathbf{k} - \mathbf{p})\frac{d\mathbf{p}}{(2\pi)^d}.$$

The equation on W_ε is thus locally in $\mathbf{x}$ and $\mathbf{k}$ given by:

$$\varepsilon\frac{\partial W_\varepsilon}{\partial t} + (\mathcal{T}_1^\varepsilon + \mathcal{T}_2^\varepsilon + \mathcal{T}_3^\varepsilon)\,W_\varepsilon + \mathcal{O}\left(\varepsilon^{3/2}\right) = 0, \tag{43}$$

where $\mathcal{T}_1^\varepsilon$ is the transport part, $\mathcal{T}_2^\varepsilon$ the collisional part, and $\mathcal{T}_3^\varepsilon$ the "inclusion" part given by

$$
\begin{aligned}
\mathcal{T}_1^\varepsilon W_\varepsilon &= P(i\mathbf{k} + \frac{\mathbf{D_y}}{2} + \frac{\varepsilon\mathbf{D_x}}{2})W_\varepsilon + W_\varepsilon P^*(i\mathbf{k} - \frac{\mathbf{D_y}}{2} - \frac{\varepsilon\mathbf{D_x}}{2}), \\
\mathcal{T}_2^\varepsilon W_\varepsilon &= \sqrt{\varepsilon}\left(\mathcal{K}_\varepsilon K\,W_\varepsilon + (1 - \gamma\chi^\delta)\mathcal{K}_\varepsilon^* W_\varepsilon\,K^*\right), \\
\mathcal{T}_3^\varepsilon W_\varepsilon &= A^\varepsilon W_\varepsilon K^* + \varepsilon B^\varepsilon W_\varepsilon K^*,
\end{aligned}
$$

where

$$P(i\mathbf{k}) = -\begin{pmatrix} 0 & c_0^2 \\ -|\mathbf{k}|^2 & 0 \end{pmatrix}.$$

24

We now expand W_ε as in (42) and equate like powers of ε in (43), using $P = P_0 + \varepsilon P_1 + \mathcal{O}(\varepsilon^2)$, $A^\varepsilon = A^0 + \sqrt{\varepsilon}A^1 + \varepsilon A^2 + o(\varepsilon)$ and $B^\varepsilon = B^0 + o(\varepsilon)$, with $A^0 = -\Delta c^2 \chi$. We do not give the expressions of A^1, A^2 and B^1 since we do not need them in the sequel. The term involving $B^\varepsilon W_\varepsilon$ is $\mathcal{O}(\varepsilon\delta^{-1})$ locally in $\mathbf{x}$ but $\mathcal{O}(\varepsilon)$ in a weak sense. We thus consider it as a term of order $\mathcal{O}(\varepsilon)$ in the expansion.

Leading order. The leading term is given by:

$$P_0(i\mathbf{k})W^0 + W^0 P_0^*(i\mathbf{k}) - \Delta c^2 \chi W^0 K^* = 0. \tag{44}$$

Introducing

$$\tilde{P}_0(\mathbf{x}, i\mathbf{k}) = -\begin{pmatrix} 0 & c_0^2 + \Delta c^2 \chi(\mathbf{x}) \\ -|\mathbf{k}|^2 & 0 \end{pmatrix},$$

we recast (44) as

$$\mathcal{L}_0 W^0 = P_0(i\mathbf{k})W^0 + W^0(\tilde{P}_0)^*(\mathbf{x}, i\mathbf{k}) = 0. \tag{45}$$

Defining $q_0(i\mathbf{k}) = |\mathbf{k}|$, the diagonalization of the matrix P_0 gives

$$\lambda_\pm(\mathbf{k}) = \pm i c_0 q_0(i\mathbf{k}), \quad \mathbf{b}_\pm(\mathbf{k}) = \frac{1}{\sqrt{2}}\begin{pmatrix} \pm i q_0^{-1}(i\mathbf{k}) \\ c_0^{-1} \end{pmatrix}, \quad \mathbf{c}_\pm(\mathbf{k}) = \frac{1}{\sqrt{2}}\begin{pmatrix} \pm i q_0(i\mathbf{k}) \\ c_0 \end{pmatrix}.$$

In the same way, concerning the matrix $\tilde{P}_0$, we have:

$$\tilde{\lambda}_\pm(\mathbf{x}, \mathbf{k}) = \pm i c(\mathbf{x}) q_0(i\mathbf{k}), \quad \tilde{\mathbf{b}}_\pm(\mathbf{x}, \mathbf{k}) = \frac{1}{\sqrt{2}}\begin{pmatrix} \pm i q_0^{-1}(i\mathbf{k}) \\ (c(\mathbf{x}))^{-1} \end{pmatrix}, \quad \tilde{\mathbf{c}}_\pm(\mathbf{x}, \mathbf{k}) = \frac{1}{\sqrt{2}}\begin{pmatrix} \pm i q_0(i\mathbf{k}) \\ c(\mathbf{x}) \end{pmatrix},$$

where $c^2(\mathbf{x}) = c_0^2 + \Delta c^2 \chi(\mathbf{x})$. We now decompose W^0 on the basis deduced from the tensorial product of eigenvectors of the matrices P_0 and $\tilde{P}_0$,

$$W^0(t, \mathbf{x}, \mathbf{k}) = \sum_{i,j=\pm} a_{i,j}(t, \mathbf{x}, \mathbf{k})\mathbf{b}_i(\mathbf{k})(\tilde{\mathbf{b}}_j(\mathbf{x}, \mathbf{k}))^*,$$

where $a_{i,j} = \mathbf{c}_i^* W_0 \tilde{\mathbf{c}}_j$. Injecting this decomposition in (45), direct calculations yield

$$a_{i,j}(t, \mathbf{x}, \mathbf{k})\left(\lambda_i(\mathbf{k}) + \overline{\tilde{\lambda}_j}(\mathbf{x}, \mathbf{k})\right) = \pm i a_{i,j}(t, \mathbf{x}, \mathbf{k})\, q_0(i\mathbf{k})\left(c_0 \pm \sqrt{c_0^2 + \Delta c^2 \chi(\mathbf{x})}\right) = 0.$$

Whence, when $i \neq j$, $a_{i,j}(t, \mathbf{x}, \mathbf{k})\left(c_0 + \sqrt{c_0^2 + \Delta c^2 \chi(\mathbf{x})}\right) = 0$, and therefore $a_{\pm,\mp} = 0$. On the other hand, when $i = j$, $a_{i,j}(t, \mathbf{x}, \mathbf{k})\left(c_0 - \sqrt{c_0^2 + \Delta c^2 \chi(\mathbf{x})}\right) = 0$. Since $\chi(\mathbf{x})$ is supported on the ball $B(\mathbf{x}_0, \mathsf{R})$, this implies that $a_{i,j}(t, \mathbf{x}, \mathbf{k}) = 0$, for $\mathbf{x} \in B(\mathbf{x}_0, \mathsf{R})$. We thus have,

$$W^0(t, \mathbf{x}, \mathbf{k}) = 0, \qquad \text{for} \quad \mathbf{x} \in B(\mathbf{x}_0, \mathsf{R}). \tag{46}$$

Thus (46) may be seen as the result of the incompatibility of the dispersion relations of the two different fields $\mathbf{u}_\varepsilon^1$ and $\mathbf{u}_\varepsilon^2$ at the inclusion location.

First order corrector. The equation for W^1 is

$$P_0(i\mathbf{k} + \frac{\mathbf{D_y}}{2})W^1 - W^1 \tilde{P}_0^*(i\mathbf{k} - \frac{\mathbf{D_y}}{2}) + \theta W^1 + \mathcal{K}_\varepsilon K\, W^0 + (1-\chi)\mathcal{K}_\varepsilon^* W_0\, K^* + A^1 W^0 K^* = 0. \tag{47}$$

Above, θ is a regularization parameter needed to ensure causality [26]. The term A^ε is supported on the ball $B(\mathbf{x}_0, \mathsf{R})$, and so is A^1. According to (46), we thus have $A^1 W^0 K^* = 0$. We introduce the Fourier transform $\hat{W}^1$ of W^1 with respect to the fast variable $\mathbf{y} \to \mathbf{p}$. Decomposing $\hat{W}^1$ as

$$\hat{W}^1(\mathbf{x}, \mathbf{p}, \mathbf{k}) = \sum_{i,j=\pm} \alpha_{i,j}(\mathbf{x}, \mathbf{p}, \mathbf{k}) \mathbf{b}_i(\mathbf{k} + \frac{\mathbf{p}}{2}) \left(\tilde{\mathbf{b}}_j(\mathbf{x}, \mathbf{k} - \frac{\mathbf{p}}{2}) \right)^*,$$

we find

$$\alpha_{i,j} = \frac{1}{2} \frac{c_0^{-2}\hat{V}^1(\mathbf{p})\lambda_i(\mathbf{k} + \frac{\mathbf{p}}{2})a_j(\mathbf{k} - \frac{\mathbf{p}}{2}) - (c)^{-2}\hat{V}^2(\mathbf{p})\tilde{\lambda}_j(\mathbf{k} - \frac{\mathbf{p}}{2})a_i(\mathbf{k} + \frac{\mathbf{p}}{2})}{\lambda_i(\mathbf{k} + \frac{\mathbf{p}}{2}) - \tilde{\lambda}_j(\mathbf{k} - \frac{\mathbf{p}}{2}) + \theta},$$

with $\hat{V}^1(\mathbf{p}) = \hat{V}(\mathbf{p})$, $\hat{V}^2(\mathbf{p}) = (1-\chi)\hat{V}(\mathbf{p})$ and therefore

$$W^1(t, \mathbf{x}, \mathbf{k}) = 0, \qquad \text{for} \quad \mathbf{x} \in B(\mathbf{x}_0, \mathsf{R}). \tag{48}$$

Transport equation. Finally, to find the equation satisfied by W^0, we use the expression (43) at the order ε:

$$\begin{aligned}
\frac{\partial W^0}{\partial t} &+ P_1(i\mathbf{k})W^0 + W^0 P_1^*(i\mathbf{k}) + A^1 W^1 + A^2 W^0 + B^0 W^0 \\
&+ (\mathcal{K}_\varepsilon K\, W^1 + (1-\gamma\chi)\mathcal{K}_\varepsilon^* W^1\, K^*) \\
&+ P_0(i\mathbf{k} + \frac{\mathbf{D_y}}{2})W^2 + W^2 \tilde{P}_0^*(i\mathbf{k} - \frac{\mathbf{D_y}}{2}) + A^0 W^2 = 0.
\end{aligned} \tag{49}$$

The terms involving $A^1 W^1$, $A^2 W^0$, and $B^0 W^0$ are equal to zero because of (46) and (48) and the fact that A^1, A^2 and B^0 are supported on the ball $B(\mathbf{x}_0, \mathsf{R})$. We still denote by $\mathbb{E}$ mathematical expectation and keep the notation a_+ for $\mathbb{E}\{a_+\}$. We assume as usual [4, 26] that

$$\mathbb{E}\left[\mathbf{c}_+^* \left(P_0(i\mathbf{k} + \frac{\mathbf{D_y}}{2})W^2 + W^2 \tilde{P}_0^*(i\mathbf{k} - \frac{\mathbf{D_y}}{2}) + A^0 W^2 \right) \tilde{\mathbf{c}}_+ \right] = 0.$$

Thus, multiplying (49) on the left by $\mathbf{c}_+^*$, on the right by $\tilde{\mathbf{c}}_+$ and integrating against a test function φ, we find that

$$\frac{\partial}{\partial t}\langle a_+, \varphi \rangle + c_0 \langle \hat{\mathbf{k}} \cdot \nabla_\mathbf{x} a_+, \varphi \rangle + \mathbb{E}\left[\langle \mathbf{c}_+^* \mathcal{L}_1 W^1 \tilde{\mathbf{c}}_+, \varphi \rangle \right] = 0, \tag{50}$$

where $\mathcal{L}_1 W^1 = \mathcal{K}_\varepsilon K\, W^1 + (1-\gamma\chi)\mathcal{K}_\varepsilon^* W^1\, K^*$. According to [4], we have

$$\mathbb{E}\left[\mathbf{c}_+^* \mathcal{L}_1 W^1 \tilde{\mathbf{c}}_+ \right] = (\Sigma(\mathbf{x}, \mathbf{k}) + i\Pi(\mathbf{x}, \mathbf{k}))\, a_+(\mathbf{k}) - \int_{\mathbb{R}^d} a_+(\mathbf{q})\sigma(\mathbf{x}, \mathbf{k}, \mathbf{q})\delta(c_0|\mathbf{q}| - c(\mathbf{x})|\mathbf{k}|)\, d\mathbf{q},$$

where

$$\Sigma(\mathbf{x}, \mathbf{k}) = \frac{\pi c_0 \tilde{c}(\mathbf{x})|\mathbf{k}|^2}{2(2\pi)^d} \int_{\mathbb{R}^d} \frac{1 + (1 - \gamma\chi(\mathbf{x}))^2}{2} \hat{R}(\mathbf{k} - \mathbf{q})\delta(c_0|\mathbf{q}| - c(\mathbf{x})|\mathbf{k}|) \, d\mathbf{q}$$

$$i\Pi(\mathbf{x}, \mathbf{k}) = \frac{1}{4(2\pi)^d}\text{p.v.} \int_{\mathbb{R}^d} \gamma\chi(\mathbf{x})(2 - \gamma\chi(\mathbf{x}))\hat{R}(\mathbf{k} - \mathbf{q}) \sum_{i=\pm} \frac{\lambda_+(\mathbf{k})\tilde{\lambda}_i(\mathbf{x}, \mathbf{k})}{\lambda_+(\mathbf{k}) - \tilde{\lambda}_i(\mathbf{x}, \mathbf{k})} d\mathbf{q}$$

$$\sigma(\mathbf{x}, \mathbf{k}, \mathbf{p}) = \frac{\pi c_0 c(\mathbf{x})|\mathbf{k}|^2}{2(2\pi)^d}(1 - \gamma\chi(\mathbf{x}))\hat{R}(\mathbf{k} - \mathbf{p}).$$

Since $a_+ = 0$ for $\mathbf{x} \in B(\mathbf{x}_0, \mathsf{R})$, we only need to know the above quantities for $\mathbf{x} \in B^c(\mathbf{x}_0, \mathsf{R})$. Then, integrating by parts the second term of (50), using again the fact that $a_+ = 0$ for $\mathbf{x} \in B(\mathbf{x}_0, \mathsf{R})$, and keeping in mind that $\chi(\mathbf{x}) = 0$ for $\mathbf{x} \in B^c(\mathbf{x}_0, \mathsf{R})$, we finally obtain that

$$\int_{B^c(\mathbf{x}_0, \mathsf{R})} \int_{\mathbb{R}^d} \left(\frac{\partial a_+}{\partial t} \varphi - c_0 \, a_+ \hat{\mathbf{k}} \cdot \nabla_{\mathbf{x}} \varphi + \Sigma(\mathbf{k}) \, a_+ \varphi - Q(a_+) \, \varphi \right) d\mathbf{x} d\mathbf{k} = 0,$$

with

$$\Sigma(\mathbf{k}) = \frac{\pi c_0^2 |\mathbf{k}|^2}{2(2\pi)^d} \int_{\mathbb{R}^d} \hat{R}(\mathbf{k} - \mathbf{q})\delta(c_0|\mathbf{q}| - c_0|\mathbf{k}|) \, d\mathbf{q},$$

$$Q(a) = \frac{\pi c_0^2 |\mathbf{k}|^2}{2(2\pi)^d} \int_{\mathbb{R}^d} \hat{R}(\mathbf{k} - \mathbf{q})a(\mathbf{q})\delta(c_0|\mathbf{q}| - c_0|\mathbf{k}|) d\mathbf{q}.$$

The above equation is nothing but the weak formulation of

$$\frac{\partial a_+}{\partial t} + c_0 \, \hat{\mathbf{k}} \cdot \nabla_{\mathbf{x}} a_+ + \Sigma(\mathbf{k}) \, a_+ = Q(a_+), \qquad \mathbf{x} \in B^c(\mathbf{x}_0, \mathsf{R}),$$

with boundary conditions

$$a_+ = 0, \qquad \mathbf{x} \in \partial B(\mathbf{x}_0, \mathsf{R}).$$

Particular case: no velocity jump $\Delta c^2 = 0$. In this configuration, W_0 does not vanish inside the inclusion. The transport equation is simply

$$\frac{\partial a_+}{\partial t} + c_0 \, \hat{\mathbf{k}} \cdot \nabla_{\mathbf{x}} a_+ + (\Sigma(\mathbf{x}, \mathbf{k}) + i\Pi(\mathbf{x}, \mathbf{k})) \, a_+ = \int_{\mathbb{R}^d} a_+(\mathbf{x}, \mathbf{q})\sigma(\mathbf{x}, \mathbf{k}, \mathbf{q})\delta(c_0|\mathbf{q}| - c_0|\mathbf{k}|) \, d\mathbf{q},$$

for all $\mathbf{x} \in \mathbb{R}^d$.

Particular case: weak velocity jump $\Delta c^2 = \mathcal{O}(\varepsilon)$. Let $\Delta c^2 = \varepsilon\widetilde{\Delta c^2}$. Following what was previously done in the general case, we obtain the transport equation

$$\frac{\partial a_+}{\partial t} + c_0 \, \hat{\mathbf{k}} \cdot \nabla_{\mathbf{x}} a_+ + (\Sigma(\mathbf{x}, \mathbf{k}) + i\Pi(\mathbf{x}, \mathbf{k})) \, a_+ + i|\mathbf{k}|\chi\frac{\widetilde{\Delta c^2}}{c_0} a_+$$
$$= \int_{\mathbb{R}^d} a_+(\mathbf{q})\sigma(\mathbf{x}, \mathbf{k}, \mathbf{q})\delta(c_0|\mathbf{q}| - c_0|\mathbf{k}|) \, d\mathbf{q}, \qquad \mathbf{x} \in \mathbb{R}^d.$$

When $\widetilde{\Delta c^2} \to \infty$, we expect to recover the general case with $a_+ = 0$ for $\mathbf{x} \in B(\mathbf{x}_0, \mathsf{R})$. To see this, let $\beta^{-1} = \widetilde{\Delta c^2} \gg 1$ and let $S(t, \mathbf{x}, \mathbf{k})$ be the solution to

$$\frac{\partial S}{\partial t} + c_0 \, \hat{\mathbf{k}} \cdot \nabla_{\mathbf{x}} S + i|\mathbf{k}|\chi c_0^{-1} = 0. \tag{51}$$

Writing a_+ as $a_+(t, \mathbf{x}, \mathbf{k}) = A(t, \mathbf{x}, \mathbf{k})e^{i\frac{S(t, \mathbf{x}, \mathbf{k})}{\beta}}$, we find that A solves

$$\frac{\partial A}{\partial t} + c_0 \, \hat{\mathbf{k}} \cdot \nabla_{\mathbf{x}} A + \left(\Sigma(\mathbf{x}, \mathbf{k}) + i\Pi(\mathbf{x}, \mathbf{k})\right) A$$
$$= e^{-i\frac{S(t, \mathbf{x}, \mathbf{k})}{\beta}} \int_{\mathbb{R}^d} A(t, \mathbf{x}, \mathbf{q})e^{i\frac{S(t, \mathbf{x}, \mathbf{q})}{\beta}}\sigma(\mathbf{x}, \mathbf{k}, \mathbf{q})\delta(c_0|\mathbf{q}| - c_0|\mathbf{k}|)\, d\mathbf{q}, \qquad \mathbf{x} \in \mathbb{R}^d.$$

According to (51), $S(t, \mathbf{x}, \mathbf{k}) \neq 0$, $\forall \mathbf{x} \in B(\mathbf{x}_0, \mathsf{R})$. Thus, as $\beta \to 0$, a_+ tends to 0 weakly in time for any $\mathbf{x} \in B(\mathbf{x}_0, \mathsf{R})$ which allows us to recover the general case. This concludes our analysis of the kinetic models to describe the correlations $\mathcal{C}^\varepsilon$ and W_ε^{12}.

B Small volume approximations in diffusive regime

We sketch here the derivation of the asymptotic formula for Dirichlet boundary conditions on the inclusion announced in Section 3.2. Let $B(\mathbf{x}_b, \mathsf{R})$ be a ball of radius R located at $\mathbf{x}_b$ and let $u_\mathsf{R} \in H^2(\Omega/\overline{B(\mathbf{x}_b, \mathsf{R})})$ be a solution to the following problem

$$-D_0\Delta u_\mathsf{R} + w\, u_\mathsf{R} = f, \qquad \mathbf{x} \in \Omega, \qquad u_\mathsf{R} = 0, \quad \mathbf{x} \in \partial B(\mathbf{x}_b, \mathsf{R}) \cup \partial\Omega,$$

where Ω is an open set in $\mathbb{R}^d$ for $d \geq 3$, $w \in \mathbb{C}$ with $\Re w \geq 0$ and $f \in L^2(\Omega)$ such that its support does not intersect $B(\mathbf{x}_b, \mathsf{R})$. Then, u_R can be extended by 0 within $B(\mathbf{x}_b, \mathsf{R})$ so that it still verifies the above equation with an additional jump condition of its normal derivative at the boundary. We denote by U the unperturbed solution, that is to say the solution when $\mathsf{R} = 0$; u_R can then be expressed in terms of U using a single layer potential and the jump condition

$$u_\mathsf{R}(\mathbf{x}) = U(\mathbf{x}) + D_0 \int_{\partial B(\mathbf{x}_b, \mathsf{R})} \left[\frac{\partial u_\mathsf{R}}{\partial n}\right](\mathbf{y})\hat{G}(w, \mathbf{x}, \mathbf{y})d\sigma(\mathbf{y}),$$

where $\hat{G}$ is the Green function, solution to $-D_0\Delta\hat{G}(w, \mathbf{x}, \mathbf{y}) + w\hat{G}(w, \mathbf{x}, \mathbf{y}) = \delta(\mathbf{x} - \mathbf{y})$ with vanishing boundary conditions on $\partial\Omega$. Let $\frac{\partial u_\mathsf{R}^-}{\partial n}$ and $\frac{\partial u_\mathsf{R}^+}{\partial n}$ be the outer and inner values of the trace of the normal derivatives at the boundary, respectively. We have $\frac{\partial u_\mathsf{R}^+}{\partial n} = 0$. Setting $u_\mathsf{R} = U + v_\mathsf{R}(\frac{\mathbf{x} - \mathbf{x}_b}{\mathsf{R}})$, the jump of the normal derivative is given by

$$\left[\frac{\partial u_\mathsf{R}}{\partial n}\right] = \left[\frac{\partial v_\mathsf{R}}{\partial n}\right] = -\frac{\partial u_\mathsf{R}^-}{\partial n} = -\frac{\partial U}{\partial n} - \frac{1}{\mathsf{R}}\frac{\partial v_\mathsf{R}^-}{\partial n},$$

and is thus or order R^{-1}. It remains to evaluate $\frac{\partial v_\mathsf{R}^-}{\partial n}$. Now v_R^- verifies:

$$v_\mathsf{R}^-(\mathbf{x}) = -U(\mathsf{R}\mathbf{x} + \mathbf{x}_b) = -U(\mathbf{x}_b) + \mathcal{O}(\mathsf{R}), \qquad \mathbf{x} \in \partial B(\mathbf{x}_b, 1).$$

Let Φ be the solution to

$$-D_0\Delta\Phi + w\Phi = 0, \qquad \mathbf{x} \in \Omega/\overline{B(\mathbf{x}_b,1)}, \qquad \Phi^- = -U(\mathbf{x}_b), \qquad \mathbf{x} \in \partial B(\mathbf{x}_b,1),$$

augmented with vanishing boundary conditions on $\partial\Omega$. Then Φ can be expressed in terms of a single layer potential so that the density η is the unique solution to

$$D_0 \int_{\partial B(\mathbf{x}_b,1)} \eta(\mathbf{y})\hat{G}(w,\mathbf{x},\mathbf{y})d\sigma(\mathbf{y}) = -U(\mathbf{x}_b), \qquad \mathbf{x} \in \partial B(\mathbf{x}_b,1).$$

Since we have $\dfrac{\partial v_{\mathsf{R}}^-}{\partial n}(\mathbf{y}) = \dfrac{\partial\Phi}{\partial n}(\mathbf{y}) + \mathcal{O}(\mathsf{R}) = \eta(\mathbf{y}) + \mathcal{O}(\mathsf{R})$, this gives thus the asymptotic expansion

$$u_{\mathsf{R}}(\mathbf{x}) = U(\mathbf{x}) - D_0\mathsf{R}^{d-2}\,\hat{M}\,\hat{G}(w,\mathbf{x},\mathbf{x}_b) + \mathcal{O}(\mathsf{R}^{d-1}),$$

where

$$\hat{M}(w) = \int_{\partial B(\mathbf{x}_b,1)} \eta(\mathbf{y})d\sigma(\mathbf{y}).$$

The relation between the time-dependent diffusion equation and the above elliptic problem is formally obtained via a Laplace transform, which yields the following time-dependent small volume expansion:

$$U_{\mathrm{cor}}(t,\mathbf{x}) = U(t,\mathbf{x}) - D_0\pi\mathsf{R}^{d-2}\int_0^t M(t-s)G(s,\mathbf{x},\mathbf{x}_b)ds + \mathcal{O}(\mathsf{R}^{d-1}),$$

where M (resp. G) is the inverse Laplace transform of $\hat{M}$ (resp. $\hat{G}$) with respect to the variable w. This concludes our analysis of the influence of small volume inclusions in the diffusive regime.

References

[1] H. AMMARI, S. MOSKOW, AND M. S. VOGELIUS, *Boundary integral formulae for the reconstruction of electric and electromagnetic inhomogeneities of small volume*, ESAIM Control Optim. Calc. Var., 9 (2003), pp. 49–66.

[2] K. AMMARI AND H. KANG, *Reconstruction of Small Inhomogeneities from Boundary Measurements*, Lecture Notes in Mathematics, Springer, Berlin, 2004.

[3] G. BAL, *Optical tomography for small volume absorbing inclusions*, Inverse Problems, 19 (2003), pp. 371–386.

[4] ——, *Kinetics of scalar wave fields in random media*, Wave Motion, 43 (2005), pp. 132–157.

[5] G. BAL, J. B. KELLER, G. C. PAPANICOLAOU, AND L. RYZHIK, *Transport theory for waves with reflection and transmission at interfaces*, Wave Motion, 30 (1999), pp. 303–327.

[6] G. BAL, G. C. PAPANICOLAOU, AND L. RYZHIK, *Self-averaging in time reversal for the parabolic wave equation*, Stochastics and Dynamics, 4 (2002), pp. 507–531.

[7] G. BAL AND O. PINAUD, *Time reversal-based imaging in random media*, Inverse Problems, 21 (2005), pp. 1593–1620.

[8] ——, *Accuracy of transport models for waves in random media*, Wave Motion, 43(7) (2006), pp. 561–578.

[9] G. BAL AND L. RYZHIK, *Diffusion Approximation of Radiative Transfer Problems with Interfaces*, SIAM J. Appl. Math., 60(6) (2000), pp. 1887–1912.

[10] G. Bal and R. Verástegui, *Time Reversal in Changing Environment*, Multiscale Model. Simul., 2(4) (2004), pp. 639–661.

[11] B. Borcea, G. C. Papanicolaou, and C. Tsogka, *Theory and applications of time reversal and interferometric imaging*, Inverse Problems, 19 (2003), pp. S139–S164.

[12] ———, *Adaptive interferometric imaging in clutter and optimal illumination*, Inverse Problems, 22 (2006), pp. 1405–1436.

[13] D. J. Cedio-Fengya, S. Moskow, and M. S. Vogelius, *Identification of conductivity imperfections of small diameter by boundary measurements. Continuous dependence and computational reconstruction*, Inverse Problems, 14 (1998), pp. 553–594.

[14] S. Chandrasekhar, *Radiative Transfer*, Dover Publications, New York, 1960.

[15] R. Dautray and J.-L. Lions, *Mathematical Analysis and Numerical Methods for Science and Technology. Vol.6*, Springer Verlag, Berlin, 1993.

[16] A. Fannjiang, *Self-averaged scaling limits for random parabolic waves*, Archives of Rational Mechanics and Analysis, 175(3) (2005), pp. 343–387.

[17] P. Gérard, P. A. Markowich, N. J. Mauser, and F. Poupaud, *Homogenization limits and Wigner transforms*, Comm. Pure Appl. Math., 50 (1997), pp. 323–380.

[18] V. Isakov, *Inverse Problems for Partial Differential Equations*, Springer Verlag, New York, 1998.

[19] A. Ishimaru, *Wave Propagation and Scattering in Random Media*, New York: Academics, 1978.

[20] E. W. Larsen and J. B. Keller, *Asymptotic solution of neutron transport problems for small mean free paths*, J. Math. Phys., 15 (1974), pp. 75–81.

[21] P.-L. Lions and T. Paul, *Sur les mesures de Wigner*, Rev. Mat. Iberoamericana, 9 (1993), pp. 553–618.

[22] D. Liu, S. Vasudevan, J. Krolik, G. Bal, and L. Carin, *Electromagnetic time-reversal imaging in changing media: Experiment and analysis*, to appear in IEEE Trans. Antennas and Prop., (2006).

[23] F. Natterer and F. Wübbeling, *Mathematical Methods in Image Reconstruction*, SIAM monographs on Mathematical Modeling and Computation, Philadelphia, 2001.

[24] J. M. Powell and J. Vanneste, *Transport equations for waves in randomly perturbed Hamiltonian systems, with application to Rossby waves*, Wave Motion, 42 (2005), pp. 289–308.

[25] J. Przybilla, M. Korn, and U. Wegler, *Radiative transfer of elastic waves versus finite difference simulations in two-dimensional random media*, J. Geoph. Res. Solid Earth, 111 (2006), p. B04305.

[26] L. Ryzhik, G. C. Papanicolaou, and J. B. Keller, *Transport equations for elastic and other waves in random media*, Wave Motion, 24 (1996), pp. 327–370.

[27] P. Sebbah, B. Hu, A. Z. Genack, R. Pnini, and B. Shapiro, *Spatial-field correlations: The building block of mesoscopic fluctuations*, Phys. Rev. Lett., 88 (2002), pp. 123901–1:123901–4.

[28] P. Sheng, *Introduction to Wave Scattering, Localization and Mesoscopic Phenomena*, Academic Press, New York, 1995.